Acta Pharmaceutica Sinica B 2024;14(3):1222−1240

Chinese Pharmaceutical Association
Institute of Materia Medica, Chinese Academy of Medical Sciences

Acta Pharmaceutica Sinica B

www.elsevier.com/locate/apsb
www.sciencedirect.com

ORIGINAL ARTICLE

GRK2 mediated degradation of SAV1 initiates hyperplasia of fibroblast-like synoviocytes in rheumatoid arthritis

Paipai Guo[a,†], Ji Jiang[a,†], Rui Chu[a], Feng He[a], Mingli Ge[a], Ruhong Fang[a], Qiuyun Guan[a], Huijuan Cheng[a], Chunru Jiang[a], Tiantian Su[a], Zhenduo Zhu[a], Hao Liu[b], Wei Wei[a,*], Shihao Zhang[a,*], Qingtong Wang[a,c,*]

[a]*Institute of Clinical Pharmacology, Anhui Medical University, Key Laboratory of Anti-inflammatory and Immune Medicine, Ministry of Education, Collaborative Innovation Center of Anti-inflammatory and Immune Medicines, Hefei 230032, China*
[b]*School of Pharmacy, Bengbu Medical College, Bengbu 233030, China*
[c]*The Third Affiliated Hospital of Anhui Medical University (the First People's Hospital of Hefei), Hefei 230061, China*

Received 19 July 2023; received in revised form 27 October 2023; accepted 29 November 2023

KEY WORDS

Rheumatoid arthritis;
Fibroblast-like synoviocytes;
G protein-coupled receptor kinase 2;
Salvador homolog-1;
Yes-associated protein

Abstract Hyperplasia and migration of fibroblast-like synoviocytes (FLSs) are the key drivers in the pathogenesis of rheumatoid arthritis (RA) and joint destruction. Abundant Yes-associated protein (YAP), which is a powerful transcription co-activator for proliferative genes, was observed in the nucleus of inflammatory FLSs with unknown upstream mechanisms. Using Gene Expression Omnibus database analysis, it was found that Salvador homolog-1 (SAV1), the pivotal negative regulator of the Hippo-YAP pathway, was slightly downregulated in RA synovium. However, SAV1 protein expression is extremely reduced. Subsequently, it was revealed that SAV1 is phosphorylated, ubiquitinated, and degraded by interacting with an important serine-threonine kinase, G protein-coupled receptor (GPCR) kinase 2 (GRK2), which was predominately upregulated by GPCR activation induced by ligands such as prostaglandin E_2 (PGE_2) in RA. This process further contributes to the decreased phosphorylation, nuclear translocation, and transcriptional potency of YAP, and leads to aberrant FLSs proliferation. Genetic depletion of GRK2 or inhibition of GRK2 by paroxetine rescued SAV1 expression and restored

*Corresponding author.
E-mail addresses: wwei@ahmu.edu.cn (Wei Wei), shihaozhang@ahmu.edu.cn (Shihao Zhang), hfwqt727@163.com (Qingtong Wang).
[†]These authors made equal contributions to this work.
Peer review under the responsibility of Chinese Pharmaceutical Association and Institute of Materia Medica, Chinese Academy of Medical Sciences.

https://doi.org/10.1016/j.apsb.2023.12.007

YAP phosphorylation and finally inhibited RA FLSs proliferation and migration. Similarly, paroxetine treatment effectively reduced the abnormal proliferation of FLSs in a rat model of collagen-induced arthritis which was accompanied by a significant improvement in clinical manifestations. Collectively, these results elucidate the significance of GRK2 regulation of Hippo-YAP signaling in FLSs proliferation and migration and the potential application of GRK2 inhibition in the treatment of FLSs-driven joint destruction in RA.

1. Introduction

The tumor-like abnormal proliferation of fibroblast-like synoviocytes (FLSs) is a critical initiator of rheumatoid arthritis (RA)[1]. Numerous studies have been conducted to explore the pathological mechanisms of FLSs hyperplasia in RA which indicate the importance of nuclear factor-κB, Janus kinase (JAK)-signal transducer and activator of transcription, and mitogen-activated protein kinase signaling induced by multiple pro-inflammatory cytokines[2–4]. Despite traditional disease-modifying anti-rheumatic drugs, tumor necrosis factor-α (TNF-α) inhibitors, and the latest JAK inhibitor treatments that effectively inhibit immune response, the activation and migration of FLSs-induced bone damage and joint deformity is still a significant clinical problem[5,6]. Therefore, a novel and critical mechanism that promotes FLSs proliferation needs to be elucidated.

Accumulating evidence has depicted that aberrant activation of Yes-associated protein (YAP), a downstream transcriptional co-activator of the Hippo pathway, stimulates cell proliferation, leading to tissue or organ hyperplasia and tumorigenesis[7]. Under normal physiological conditions, activation of upstream Salvador homolog1 (SAV1)[8], mammalian Ste20-like 1 and 2 (MST1/2)[7], large tumor suppressor 1 and 2 (Lats1/2)[9], and MOB kinase activator 1 (MOB1) in the Hippo pathway promotes YAP phosphorylation and degradation. The inhibition of Hippo signaling promotes YAP's nuclear translocation, where it binds to TEA domain transcription factor1/4 (TEAD1/4) to induce the transcription of genes involved in proliferation and migration, such as connective tissue growth factor (CTGF) and cysteine-rich inducer of angiogenesis 61 (Cyr61)[9]. Previous work has determined that nuclear expression of YAP was present in synovial linings with hyperplasia, whereas YAP expression was barely discernible in non-proliferative or normal synovial linings[10]. Verteporfin, an inhibitor of the YAP-TEAD binding interaction, ameliorates the severity of K/BxN serum-transfer arthritis in mice[11]. Although previous studies have implicated YAP in the progression of arthritis, there are still some important connections that need to be established, such as changes in YAP activity across different species of FLSs, the correlation between altered YAP activity and abnormal proliferation of FLSs, and the mechanisms by which upstream pro-inflammatory factors regulate YAP. SAV1, a known tumor suppressor in various cancer types, exhibits downregulation in cancerous tissues or cells, thereby promoting tumor progression, cancer aggressiveness, and unfavorable prognosis[8,12]. However, SAV1 downregulation has not been investigated in RA, with the mechanism of expression and regulation of SAV1 in many diseases including RA remaining ambiguous. Here, a systematic investigation of the regulatory mechanisms and functional role of SAV1 in inflammatory FLSs was performed to elucidate the role of SAV1 in RA.

G protein-coupled receptor kinase 2 (GRK2) is a serine/threonine protein kinase that is widely distributed throughout the body[11]. It is a multi-domain protein involved in various cellular functions, including cell proliferation and migration, cell cycle regulation, cardiac contraction, vasodilation and generation, as well as inflammation[13,14]. Dysregulation of GRK2 is implicated in various human diseases, including secondary progressive multiple sclerosis, RA, cardiovascular disease, and cancers[13,15]. Our previous studies have indicated that GRK2 is highly expressed in the synovium of RA patients and animal models of arthritis, in which increased levels of GRK2 are involved in the abnormal proliferation of FLSs. Moreover, targeted inhibition of GRK2 can prevent and ameliorate arthritis[16]. This evidence suggests that GRK2 plays a crucial role in the abnormal proliferation of FLSs, which leads to arthritis. However, further studies are needed to confirm this hypothesis. Therefore, understanding the regulatory network of GRK2 is essential for comprehending the mechanism behind FLSs proliferation.

Data presented here depict that SAV1 is downregulated in both human RA and rat arthritis, and overexpression of SAV1 inhibits the proliferation and migration of FLSs. Mechanistically, the interaction between GRK2 and SAV1 promotes the nuclear translocation of YAP and drives hyperplasia of FLSs. Our findings identify the GRK2-SAV1-YAP signaling axis as an FLSs-specific therapeutic target in RA synovitis.

2. Materials and methods

2.1. Patients and specimens

RA synovium was obtained from RA patients who received surgical synovectomy of the knee, while normal synovium was collected from donors without a history of RA who underwent lower limb amputation due to traffic accidents. These procedures were approved by the Biomedical Ethics Committee of Anhui Medical University (Approval No: 20200609, Hefei, China), and informed consent from patients was acquired.

2.2. Animals

SD rats (male, 200 ± 20 g), aged 6−8 weeks were procured from Zhejiang Vital River Laboratory Animal Technology Co. Ltd. (Jiaxing, China). Heterozygous knockout GRK2 ($GRK2^{+/-}$) mice (male, 20 ± 4 g) between 6 and 8 weeks were designed by our group and constructed by the Model Animal Research Center of

Nanjing University (Nanjing, China)[17]. Heterozygous mice were implemented in the study since the homozygous GRK2 gene deletion is lethal. All animals were housed in the specific pathogen-free (SPF) animal laboratory of Anhui Medical University (Hefei, China), in compliance with ARRIVE and NIH guidelines for laboratory animal care and use. The Ethics Review Committee for Animal Experimentation of Anhui Medical University approved these experiments (No: PZ-2020-005, Hefei, China).

2.3. Inducing and treating the collagen induced arthritis (CIA) model in rats

Chicken type II collagen (Chondrex, Redmond, WA, USA) was mixed with Freund's complete adjuvant containing 4 mg/mL heat-denatured mycobacterium (Chondrex) to prepare an emulsion. On Day 0, the emulsion was injected intracutaneously into the toes and tail roots of rats to establish the CIA rat model. On Day 7, the rats were challenged in the same manner. After presenting secondary joint swelling on Day 14, the CIA rats were randomly divided into vehicle-treated CIA group (CIA-Veh), 2.5 mg/kg/day of indomethacin (Linfen Qilin Pharmaceutical Co., Ltd., Linfen, China) treated group (CIA-Indo), 15 mg/kg/day of Paroxetine (China-US Tianjin Shike Pharmaceutical, Tianjin, China) treated group (CIA-PAR) and 0.5 mg/kg/3 day of methotrexate (MTX) (Tonghua Maoxiang Pharmaceutical, Tonghua, China) treated group (CIA-MTX) and treated for 14 days. Body weight change, global assessment, arthritis index, swollen joints count, and secondary paw swelling were assessed every three days by two blinded, independent observers.

2.4. Induction of collagen antibody induced arthritis (CAIA) model

On Day 0, GRK2$^{+/-}$ mice and wild-type C57BL/6 littermates were intraperitoneally injected with 5 mg of type II collagen antibody (#53100, Chondrex, Redmond). On Day 3, an abdominal injection of 50 μg lipopolysaccharide was administered to enhance stimulation[18].

2.5. Thymus index and spleen index calculation

Rats were weighed and the thymus and spleen were excised for weighing. Spleen or thymus index calculated as a percentage of body weight, spleen or thymus weight (g)/body weight (g) × 100.

2.6. Histopathological examination

The secondary swollen ankle joints of the rats were fixed in formalin for 24 h and then decalcified in 10% ethylene diamine tetraacetic acid (EDTA) (#E671001-0500, Sangon Biotech (Shanghai) Co., Ltd., Shanghai, China). The paraffin-embedded joints were sectioned and stained with hematoxylin and eosin (H&E). Pathological changes in the joints are graded from 0 (no pathological change) to 4 (severe pathological change) based on five aspects including inflammation, pannus formation, cartilage erosion, cellular infiltration, and synoviocyte proliferation.

2.7. Cell proliferation and migration determination

The human FLSs cell line MH7A, purchased from JENNIO Biological Technology (Guangzhou, China), was cultured in DMEM (#01-100-1ACS, Biological Industries, Kibbutz Beit Haemek, Israel) medium with 10% fetal bovine serum (FBS) (#04-001-1A, Biological Industries) at 37 °C in a 5% CO_2 incubator. The primary rat FLSs were obtained from the knee joints of rats through synovial tissue block culture.

The cell suspension obtained after digestion was transferred into a 96-well plate (3×10^4 cells/well). Cells were cultured overnight in 5% FBS and then treated with verteporfin (VP) (#129497-78-5, Selleck Chemicals, Houston, TX, USA), PGE_2 (#363-24-6, Cayman Chemical, Ann Arbor, MI, USA), H89 (#HY-15979A, MedChemExpress LLC., Monmouth Junction, NJ, USA), or paroxetine (#P9623, Sigma−Aldrich Pty Ltd., St. Louis, MO, USA) for 24 h. The plate was washed with PBS and fixed with 4% formaldehyde and stained with DAPI (#C1005, Beyotime, Shanghai, China) before fluorescent images were captured and cell number was counted using a High-Content Imaging system (ImageXpress Micro-4, Molecular Devices LLC., San Jose, CA, USA)[15].

For migration determination, normal or *in vivo* treated-FLSs or FLSs transfected with GRK2 siRNA (si-GRK2), control siRNA (si-NC), flag vector, or flag-SAV1 with 100 μL serum-free medium were added into the upper chamber of a Transwell plate (#3378, Corning Incorporated, NY, USA) and 500 μL of 10% FBS medium was added into the lower chamber. In indicated experiments, cells pretreated with VP or paroxetine, or with prostaglandin E_2 (PGE_2) were added into the lower chamber as a stimulant. 24 h later, the upper chamber was stained with 0.2% crystal violet for 30 min, and five images were taken using an inverted microscope (Olympus, Tokyo, Japan) to count the number of migrated cells. The relative ability of cell migration was then calculated by normalizing the number of migrated cells in each group to the control group.

2.8. Immunofluorescence

FLSs (4×10^5 cells/well) were grown and treated as described above in individual experiments on sterile glass coverslips in 24-well plates. The plate was washed three times with PBS and fixed with 4% paraformaldehyde for 20 min. Cells were then permeabilized with 0.5% Triton X-100 (#P-0096, Beyotime, Shanghai, China) for 5 min and blocked with 5% bovine serum albumin (BSA) (#ST025-5g, Beyotime) for 1 h. Alternatively, synovial tissue sections from RA patients or treated CIA rats were dewaxed, rehydrated, and permeabilized with 0.05% Triton-X 100 for 30 min. Antigen retrieval was performed on the tissue using EDTA antigen retrieval solution (#ZSGB-BIO, Beijing, China) for 10 min followed by a 1 h-blocking in 5% BSA. The coverslips or tissue sections were then incubated with primary antibodies at 4 °C overnight, followed by the staining of fluorescently conjugated secondary antibodies. The primary and secondary antibodies were listed in Supporting Information Tables S1 and S2. After being incubated with DAPI, the coverslips and sections were mounted onto a glass slide and imaged on a Leica TCS SP8 confocal microscope (Leica Microsystems, Wetzlar, Germany). The mean fluorescence intensity (MFI) of YAP in the nucleus (N) and in the cytoplasm (C) was compared and the percentage of cells with N < C, N=C, or N > C YAP expression was analyzed.

2.9. Immunohistochemistry (IHC)

Paraffin-embedded synovium sections were subjected to IHC for YAP analysis. The sections were firstly dewaxed with xylene and rehydrated in a series of graded ethanol solutions and then were

heated in EDTA (pH = 8.0) for 30 min for antigen retrieval. Subsequently, the tissues were incubated overnight at 4 °C with rabbit anti-YAP (1:200), followed by the incubation of enzyme-labeled sheep anti-mouse/rabbit IgG polymer (PV-9000, ZSGB-BIO, Beijing, China) for 30 min at room temperature, diaminobenzidine (DAB) (#ZLI-9018, ZSGB-BIO) substrate was added for coloration. Finally, the slides were counterstained with hematoxylin and sealed.

2.10. Separation of total, cytoplasmic and nuclear protein of FLSs

For total protein extraction, cells were lysed on ice with RIPA lysis buffer (#P0013B, Beyotime, Shanghai, China) supplemented with phosphatase inhibitors (#P1081, Beyotime) and protease inhibitors (#ST506, Beyotime). After incubation for 30 min at 4 °C, the total protein was obtained by centrifugation at 12,000 $\times g$ for 10 min. Cytoplasmic and nuclear proteins were extracted using a nuclear protein extraction kit (#P0027, Beyotime) following the manufacturer's instructions. Briefly, cells were suspended in Cytoplasmic Protein Extraction Reagent A and incubated at 4 °C for 15 min. The mixture was centrifuged at 16,000 $\times g$ for 5 min at 4 °C, and the resulting supernatant contained the extracted cytoplasmic protein. To extract nuclear protein from the pellet, spin by suction was implemented to completely remove the supernatant. The pellet was resuspended in nuclear protein extraction buffer and incubated with constant shaking for 30 min at 4 °C. The supernatant after centrifugation at 16,000 $\times g$ for 10 min at 4 °C contained the nuclear protein.

2.11. Immunoblotting

The extracted protein was mixed with loading buffer and separated by electrophoresis in 10% SDS-polyacrylamide gels. The separated proteins were then transferred onto PVDF membranes (#IPVH00010, Merck Millipore, Billerica, MA, USA) and blocked with Tris-Tween-20 (TBST) buffer containing 5% non-fat milk for 1 h at 37 °C. The membranes were incubated overnight at 4 °C with the appropriate antibody. After being washed with TBST, the membranes were incubated with the corresponding horseradish peroxidase-conjugated secondary antibodies for 2 h at 37 °C. All the primary antibodies and secondary antibodies were listed in Tables S1 and S2. The bands were then displayed with Immobilon Western Chemiluminescent HRP Substrate (#WBKLS0100, EMD Millipore Corporation, Burlington, MA, USA) and captured on an ImageQuant LAS 4000 Micro Instrument (GE Healthcare Bio-Science AB, Uppsala, Sweden). The mean grey value of the protein samples was quantified using Image J. In the phos-tag assay, MH7A cells were transfected with indicated plasmids or treated with paroxetine. 48 h post-transfection, cells were lysed and immunoprecipitated with anti-Flag antibody. Phosphorylation of SAV1 proteins was detected using gels containing phos-tag Acrylamide AAL-107 (#304-93521, FUJIFILM Wako Pure Chemical Corporation).

2.12. Cycloheximide (CHX) chase assay

CHX (#HY-12320, MedChemExpress LLC., Monmouth Junction, NJ, USA), a protein synthesis inhibitor was used to evaluate the stability of SAV1 at 0, 1, 3, 6, 9, or 12 h. Alternatively, MH7A cells were pretreated with proteasome inhibitor MG-132 (#HY-13259, MedChemExpress LLC.) or paroxetine for 8 h before to the CHX treatment. Immunoblotting was performed to detect the expression level of SAV1 protein.

2.13. Real-time qPCR

The mRNA expressions of CTGF and Cyr61 were detected using real-time qPCR. Total RNA was extracted with TRIzol reagent (#267309, Life Technologies Corporation, Carlsbad, CA, USA). The isolated mRNA was reversely transcribed into cDNA using the PrimeScript RT Kit (#RR037A, TaKaRa, Tokyo, Japan) according to the manufacturer's instructions. Real-time PCR was performed using the TB Green Premix Ex Taq II Kit (#RR820A, TaKaRa), and data were collected on an Applied Biosystems 7500 Real-Time PCR System (Life Technologies Corporation). The relative amount of individual mRNA level was normalized to GAPDH level, and quantified by the $2^{-\Delta\Delta Ct}$ method. The primer sequences were listed in Supporting Information Table S3.

2.14. Transfection of small interfering RNA (siRNA) and plasmids

GRK2, SAV1, and YAP siRNAs were chemically synthesized by General biological co., Ltd. (Anhui, China) to knock down gene expression in rat FLSs or MH7A cells. When rat FLSs or MH7A cells reached 60%−70% confluency in 6-well plates, the cells were transfected with siRNA by applying Lipofectamine 3000 (#L3000015, Thermo Fisher Scientific, Waltham, MA, USA) according to the manufacturer's protocol. The deletion was confirmed by immunoblotting after 48 h. The sequences of the siRNA were listed in Supporting Information Table S4. MH7A cells were seeded into 10 cm dishes and transfected with HA-vector, Flag-vector, HA-GRK2, Flag-SAV1, Flag-YAP, and/or Myc-Ub as indicated with Lipofectamine 3000.

2.15. Co-immunoprecipitation assay

Cells were seeded in a 10 cm dish and treated as described. Then the cells were washed three times with PBS and lysed in lysis buffer (25 mmol/L HEPES, 5 mmol/L EDTA, 150 mmol/L NaCl, 1% Triton X-100, 10% (*v*/*v*) glycerin and protease inhibitors) for 30 min on ice. Cell lysates were centrifuged at 15,000 $\times g$ for 15 min. The lysate was precleaned by IgG-coated protein A/G plus-agarose beads (sc-2003, Santa Cruz, CA, USA) and then mixed with the indicated primary antibody-coated beads and incubated overnight at 4 °C. The immune complexes were collected by spin and eluted with 5 × SDS loading buffer, which were then subjected to immunoblotting.

2.16. Mass spectrometry

HEK293T cells were transfected with Flag-vector or Flag-SAV1. Flag was immunoprecipitated as described above, and IgG served as the control group. After electrophoretic separation of the immunoprecipitated proteins, excised gel fragments were digested by in-gel trypsin digestion and dried, then dissolved in 0.1% formic acid, and auto-sampled directly on a C18 PepMap (75 μm × 15 cm, 2 μm, 100 Å). Samples were eluted in a linear gradient of 3%−35% acetonitrile in 0.1% formic acid for 60 min at a flow rate of 300 nL/min. Mass spectrometry data were obtained by using the Orbitrap Fusion Lumos mass spectrometer (Thermo Fisher Scientific, Waltham, MA, USA). The Thermo Fisher RAW files were imported into Proteome Discoverer v3.0

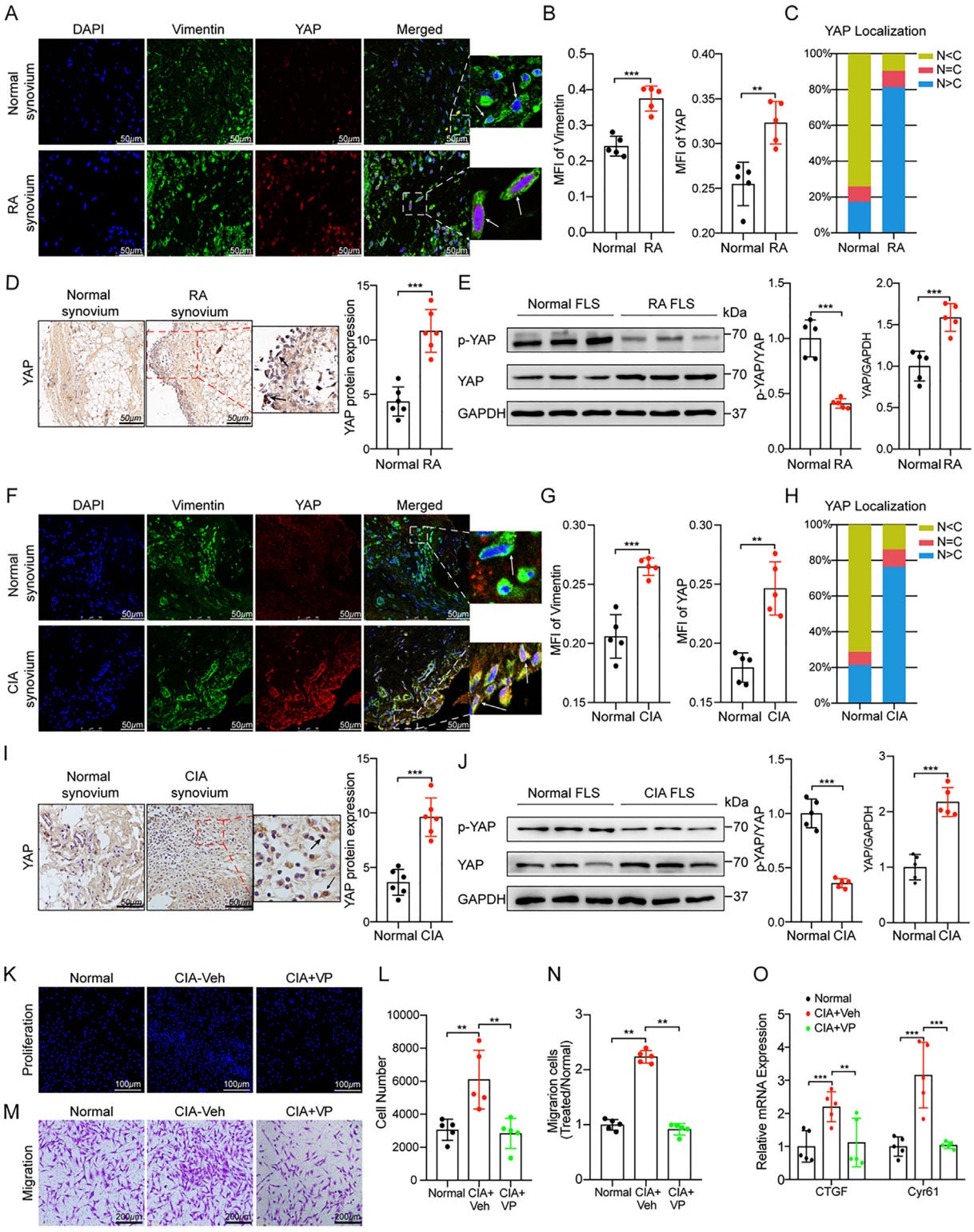

Figure 1 Expression of YAP in the inflammatory synovium or FLSs. (A) Paraffin sections of human synovium were stained for vimentin (green) and YAP (red). Images were taken by confocal microscope. Scale bar, 50 μm. White arrow: positive vimentin and YAP staining in FLSs. (B) The MFI of Vimentin and YAP was analyzed by ImageJ software ($n = 5$). (C) The distribution analysis graph of YAP in 200 randomly selected cells was displayed. (D) Representative IHC images reveal the protein expression of YAP in human synovium ($n = 6$). Scale bars, 50 μm. Black arrow: positive YAP staining in FLSs. (E) The expression of phospho-YAP and total YAP in the human FLSs was detected by immunoblotting ($n = 5$). (F) Paraffin sections of rat synovium stained for vimentin (green) and YAP (red). Images were taken by confocal microscope. Scale bar, 50 μm. White arrow: positive vimentin and YAP staining in FLSs. (G) The MFI of Vimentin and YAP was analyzed by ImageJ software ($n = 5$). (H) The distribution analysis graph of YAP in 200 randomly selected cells was plotted. (I) Representative IHC images depict the protein

for independent searches against the UniProt database. The criteria for protein identification require a false discovery rate of no more than 1% and at least 1 peptide match per protein.

2.17. Bioinformatic data mining

Analysis of SAV1 mRNA expression in RA synovium and control samples was conducted utilizing the GSE55235[19] and GSE2053[20] datasets from the Gene Expression Omnibus (GEO) database. Volcano plots were generated to visualize the expression data of each microarray probe, with relative fold change (logFC, RA *versus* Normal) plotted on the *x*-axis, and *P* value (−10log (*P*-value)) plotted on the *y*-axis.

2.18. Statistical analysis

GraphPad Prism 8.0.0 was used for data processing and statistical analysis, and the results are presented as mean ± SD. Differences between two groups of data were compared using independent *t*-tests, and differences among multiple groups of data were compared using one-way analysis of variance (ANOVA) with Tukey's post-test. Two-way-ANOVA followed by Tukey's multiple comparisons test was applied to compare differences between groups of data with 2 variables. $P < 0.05$ was considered statistically significant.

3. Results

3.1. YAP is upregulated in inflammatory FLSs and is associated with the proliferation and migration of FLSs

The specific role of the Hippo pathway in the aberrant proliferation of RA FLSs remains elusive. Abnormal activation of YAP is frequently observed in human cancers, where tumor cells exploit aberrant YAP or nuclear translocation to promote their proliferation, migration, and metastasis[21]. To determine the subcellular localization of YAP in RA FLSs, immunofluorescence of synovium sections from both normal individuals and RA patients was performed (Fig. 1A). Compared to normal controls, the expression levels of vimentin, a biomarker for FLSs, and YAP were significantly increased in the synovium of RA patients (Fig. 1B). Notably, YAP was predominantly localized within the nucleus of RA synovium (Fig. 1C) and IHC also revealed stronger YAP staining in RA tissue than in normal tissue (Fig. 1D). The synovial tissue was cultured using the tissue block adherence method to obtain FLSs. More total YAP, but less phosphorylated YAP was found in RA FLSs (Fig. 1E). Consistent with findings in human samples, synovium collected from rats at the peak of inflammation on Day 29 of the CIA rat arthritis model (Supporting Information Fig. S1A−E) depicted significantly upregulated YAP abundance that was predominantly localized in the nucleus (Fig. 1F−I). Moreover, an increase in YAP protein level and a decrease in its phosphorylation were detected in the FLSs from CIA rats using immunoblotting (Fig. 1J). To further clarify the role of YAP in inflammatory FLSs, FLSs from CIA rats were subjected to *in vitro* treatment with a YAP-TEAD binding inhibitor VP, which significantly suppressed the increased proliferation and migration of FLSs in the CIA group, resulting in cell numbers similar to those observed in normal rats after 24 h of culture (Fig. 1K−N). Compared to the CIA group, VP significantly reduced the YAP fluorescence intensity (Fig. S1F and S1G) and inhibited its nuclear distribution (Fig. S1H). It has been demonstrated that YAP binding to TEAD is capable of enhancing the transcriptional activation of target genes, such as CTGF and Cyr61, under pathological conditions. This ultimately promotes fibroblast proliferation and migration, leading to tissue fibrosis[22,23]. The mRNA levels of CTGF and Cyr61 were hence quantified by qPCR in each group, revealing a significant upregulation of both transcripts in the CIA group compared to normal controls. Importantly, VP treatment significantly reduced the expression of both genes within the CIA cohort (Fig. 1O). The function of YAP on the growth and metastasis of MH7A cells was therefore examined. Overexpression of YAP with Flag-YAP transfection (Supporting Information Fig. S2A) greatly promoted cell proliferation and migration (Fig. S2B and S2C). On the contrary, when YAP expression was knocked down by specific siRNA (Fig. S2D), the proliferation and migration of MH7A cells were significantly inhibited (Fig. S2E and S2F). Together, these data suggest that increased YAP expression or the interaction of YAP with TEAD promotes aberrant proliferation and migration of FLSs, confirming YAP functions as a promoter for FLSs hyperplasia and inflammatory arthritis development.

3.2. SAV1 is downregulated in inflammatory FLSs and correlates with FLSs proliferation and migration

To further elucidate the specific component of Hippo signaling that is modulated in RA, a comparative analysis of genetic alterations was conducted between RA and normal synovium in datasets obtained from GEO (GSE55235, GSE2053). Volcano plots generated to visualize the expression data of each microarray probe, with relative fold change (logFC, RA *versus* Normal) plotted on the *x*-axis, and *P* value (−10log (*P*-value)) plotted on the *y*-axis (Fig. 2A) revealed that SAV1 mRNA was significantly downregulated in RA tissues compared with that of normal synovium (Fig. 2B). No significant differences in the mRNA levels of other Hippo signaling members including MST1, MST2, Lats1 and YAP were observed between normal and RA synovium in the database (Supporting Information Fig. S3A−D). Then the GEO data was validated by qPCR using isolated FLSs and displayed that SAV1 was downregulated and YAP was elevated in RA FLSs, but not MST1, MST2, Lats1, and Lats2 (Fig. 2C; Fig. S3E−I). Additionally, the inflammatory FLSs exhibited a

expression of YAP in CIA rat synovium ($n = 6$). Scale bars, 50 μm. Black arrow: positive YAP staining in FLSs. (J) Expression of phospho-YAP, total YAP in rat FLSs was detected by immunoblotting ($n = 5$). (K, L) FLSs from CIA rats were treated with VP (5 μmol/L) for 24 h, and nuclei were labeled with DAPI. Images were captured with a high-content cell imager and the number of cells was counted ($n = 5$). Scale bar, 100 μm. (M, N) FLSs of CIA rats were treated with VP (5 μmol/L) for 24 h and visualized by crystal violet staining ($n = 5$). Scale bar, 200 μm. (O) FLSs of CIA rats were treated with VP (5 μmol/L) for 24 h, and the transcription levels of the YAP downstream genes CTGF and Cyr61 were examined by real-time qPCR ($n = 5$). All data were presented as mean ± SD, and were analyzed by *t*-tests or one-way ANOVA followed by a Tukey's post-test, $^{**}P < 0.01$, $^{***}P < 0.001$.

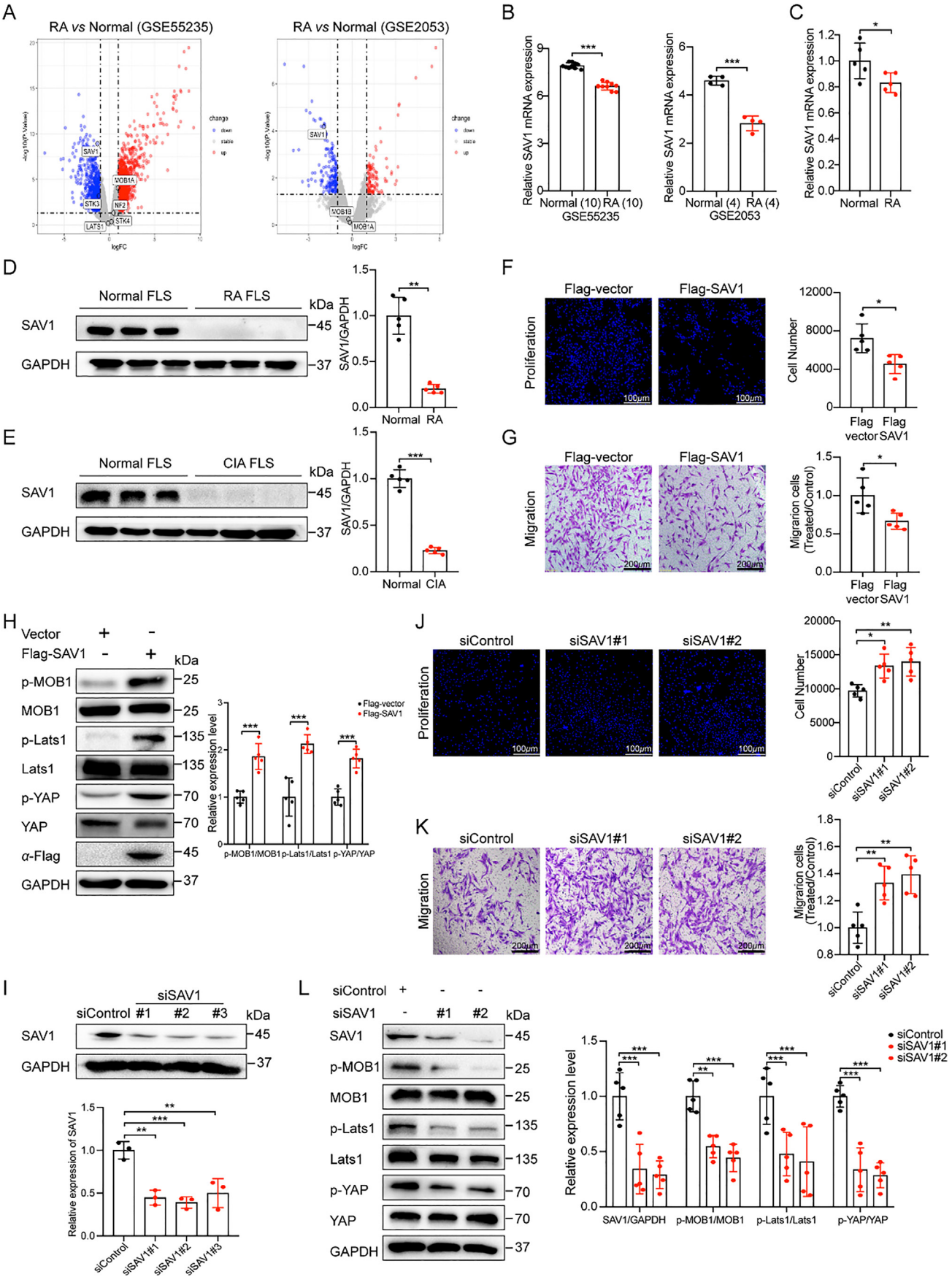
A
RA vs Normal (GSE55235)
RA vs Normal (GSE2053)
SAV1
MOB1A
STK3
NF2
LATS1
STK4
MOB1B
MOB1A
change
down
stable
up
-log10(P.Value)
logFC
B
Relative SAV1 mRNA expression
Normal (10) RA (10)
GSE55235
Normal (4) RA (4)
GSE2053
C
Relative SAV1 mRNA expression
Normal RA
D
Normal FLS
RA FLS
kDa
SAV1
GAPDH
45
37
SAV1/GAPDH
Normal RA
E
Normal FLS
CIA FLS
kDa
SAV1
GAPDH
45
37
SAV1/GAPDH
Normal CIA
F
Flag-vector
Flag-SAV1
Proliferation
100μm
Cell Number
Flag vector
Flag SAV1
G
Flag-vector
Flag-SAV1
Migration
200μm
Migrarion cells (Treated/Control)
Flag vector
Flag SAV1
H
Vector + -
Flag-SAV1 - +
kDa
p-MOB1
MOB1
p-Lats1
Lats1
p-YAP
YAP
α-Flag
GAPDH
25
25
135
135
70
70
45
37
Relative expression level
Flag-vector
Flag-SAV1
p-MOB1/MOB1
p-Lats1/Lats1
p-YAP/YAP
J
siControl
siSAV1#1
siSAV1#2
Proliferation
100μm
Cell Number
siControl
siSAV1#1
siSAV1#2
K
siControl
siSAV1#1
siSAV1#2
Migration
200μm
Migrarion cells (Treated/Control)
siControl
siSAV1#1
siSAV1#2
I
siSAV1
siControl #1 #2 #3
kDa
SAV1
GAPDH
45
37
Relative expression of SAV1
siControl
siSAV1#1
siSAV1#2
siSAV1#3
L
siControl + - -
siSAV1 - #1 #2
kDa
SAV1
p-MOB1
MOB1
p-Lats1
Lats1
p-YAP
YAP
GAPDH
45
25
25
135
135
70
70
37
Relative expression level
siControl
siSAV1#1
siSAV1#2
SAV1/GAPDH
p-MOB1/MOB1
p-Lats1/Lats1
p-YAP/YAP

Table 1 Proteins interacting with SAV1 in mass spectrometry.

Protein	Peptide
Serine/threonine-protein kinase 4 (STK4/MST1)[a]	9
LIM domain and actin-binding protein 1 (LIMA1)	8
POTE ankyrin domain family member E (POTEE)	8
Unconventional myosin-Id (MYO1D)	8
Kelch-like protein 22 (KLHL22)	7
BAG family molecular chaperone regulator 2 (BAG2)	7
Serine/threonine-protein kinase 3 (STK3/MST2)[a]	7
Beta-adrenergic receptor kinase 1 (GRK2)	6
Lamin-B receptor (LBR)	5
Maleylacetoacetate isomerase (GSTZ1)	4
Tropomodulin-3 (TMOD3)	4
Plectin (PLEC)	3
Collagen alpha-1(I) chain (COL1A1)	3
Calmodulin-1 (CALM1)	2
Angiomotin (AMOT)[a]	2
Serine/arginine-rich splicing factor 10 (SRSF10)	2
ATP-binding cassette sub-family F member 2 (ABCF2)	2
Superkiller viralicidic activity 2-like 2 (SKIV2L2)	2

[a]Known SAV1-interacting partner.

significant reduction in SAV1 protein levels (Fig. 2D and E). When Flag-SAV1 was overexpressed in MH7A cells through transduction, the resulting impact on cellular function was that Flag-SAV1 inhibited both cell proliferation and migration (Fig. 2F and G). Further, immunoblotting determined that SAV1 overexpression promoted the phosphorylation of MOB1, Lats1, and YAP (Fig. 2H). To confirm that SAV1 downregulation is a key factor in promoting FLSs proliferation, MH7A cells were transfected with specific SAV1 siRNA (Fig. 2I), and cell proliferation was determined using a high-content cell imaging assay. Silencing SAV1 in MH7A cells significantly enhanced the proliferation of MH7A cells (Fig. 2J). Transwell migration assay revealed an improved migratory ability of MH7A cells when lacking SAV1 (Fig. 2K). The downregulation of SAV1 also inhibited the phosphorylation of MOB1, Lats1, and YAP (Fig. 2L). Collectively, these experiments indicate that SAV1 effectively inhibits both growth and migration of MH7A cells while promoting phosphorylation of YAP and its upstream effectors, strongly suggesting that SAV1 functions as a proliferation suppressor in RA FLSs.

3.3. GRK2 interacts with SAV1 and induces SAV1 phosphorylation, ubiquitination and degradation

As detected in inflammatory FLSs, the protein levels of SAV1 changed more significantly than the mRNA levels, indicating that certain proteins may affect the degradation process of SAV1. To identify proteins that interact with SAV1, immunoprecipitation followed by mass spectrometry sequencing was performed. The enrichment of several proteins including previously reported interactors MST1/2[24] and AMOT[25] were observed. Among the novel interactions of SAV1, it was found that GRK2, a serine/threonine protein kinase, has a significant binding interaction (Table 1; Supporting Information Fig. S4A). We have previously demonstrated that GRK2 plays a crucial role as a negative regulator of GPCR signaling in FLSs[26], with GRK2 expression being significantly increased in inflammatory FLSs (Fig. 3A), and its expression correlated positively with synovitis severity[15]. To investigate the mechanisms underlying GRK2-mediated regulation of Hippo-YAP signaling in RA FLSs, the potential interaction between GRK2 and SAV1 was explored. Co-immunoprecipitation assays depicted a constitutive interaction between endogenous GRK2 and SAV1 in MH7A cells (Fig. 3B). Consistent with these results, exogenous interaction between SAV1 and GRK2 was also observed in MH7A cells when co-transfected with Flag-SAV1 and HA-GRK2 (Fig. 3C and D). Up-regulation of GRK2 in MH7A cells inhibited the phosphorylation of MOB1, Lats1, and YAP. Surprisingly, overexpression of GRK2 suppressed the protein levels of SAV1 (Fig. 3E). Hence, the mechanism by which GRK2 promotes the degradation of SAV1 was further investigated. Specifically, GRK2 functions as a kinase, and its overexpression significantly enhances the phosphorylation level of SAV1. Notably, treatment with the GRK2 inhibitor paroxetine[27] markedly suppresses SAV1 phosphorylation (Fig. 3F). To investigate the impact of GRK2 on SAV1 ubiquitination and subsequent degradation, MH7A cells were co-transfected with Flag-SAV1, HA-GRK2, and Myc-Ub. The findings from these experiments demonstrate that the upregulation of GRK2 significantly enhances SAV1 ubiquitination. Furthermore, proteasome inhibitor MG-132 treatment promoted the ubiquitination of SAV1 in the presence of GRK2, while paroxetine inhibited SAV1 ubiquitination (Fig. 3G; Fig. S4B). To evaluate the impact of GRK2 on the post-translational stability of SAV1,

Figure 2 SAV1 is involved in MH7A cell proliferation and migration *in vitro*. (A) Volcano plots compared RA and normal synovium analyses, with differential expression plotted along the *x*-axis in LogFC and statistical significance plotted along the *y*-axis in $-10\log(P\text{-value})$. Down-regulated genes are colored blue, up-regulated genes are colored red, and stable genes are colored grey. Selected genes with changes in Hippo pathway members were highlighted with black spots. (B) The levels of SAV1 mRNA in RA and normal synovium from GEO (GEO accession numbers: GSE55235 and GSE2053) were compared. (C) The mRNA expression of SAV1 was detected in human FLSs by real-time qPCR ($n = 5$). (D) The protein expression of SAV1 was detected in human FLSs and rat FLSs by immunoblotting ($n = 5$). (E) The expression of SAV1 protein was detected in human and rat FLSs by immunoblotting ($n = 5$). (F) MH7A cells were transfected with Flag-vector or Flag-SAV1 for 48 h, and nuclei were labeled with DAPI. Images were captured with a high-content cell imager and the number of cells was counted ($n = 5$). Scale bar, 100 μm. (G) MH7A cells were transfected with Flag-vector or Flag-SAV1 for 48 h, visualized by crystal violet staining ($n = 5$). Scale bar, 200 μm. (H) MH7A cells were transfected with Flag-vector or Flag-SAV1 for 48 h, and immunoblotting was performed using antibodies against the indicated proteins ($n = 5$). (I) SAV1 siRNA was transfected into MH7A, and the inhibition rate of SAV1 was detected by immunoblotting ($n = 3$). (J) The SAV1 gene was silenced by siRNA in MH7A cells for 48 h. Nuclei were labeled with DAPI and images were captured with a high-content cell imager ($n = 5$). Scale bar, 100 μm. (K) The SAV1 gene was knocked down by siRNA in MH7A cells for 48 h and visualized by crystal violet staining ($n = 5$). Scale bar, 200 μm. (L) The SAV1 gene was knocked down by siRNA in MH7A cells for 48 h and immunoblotting was performed using antibodies against the indicated proteins ($n = 5$). All data were presented as mean ± SD, and were analyzed by *t*-tests or one-way ANOVA followed by a Tukey's post-test, $^*P < 0.05$, $^{**}P < 0.01$, $^{***}P < 0.001$.

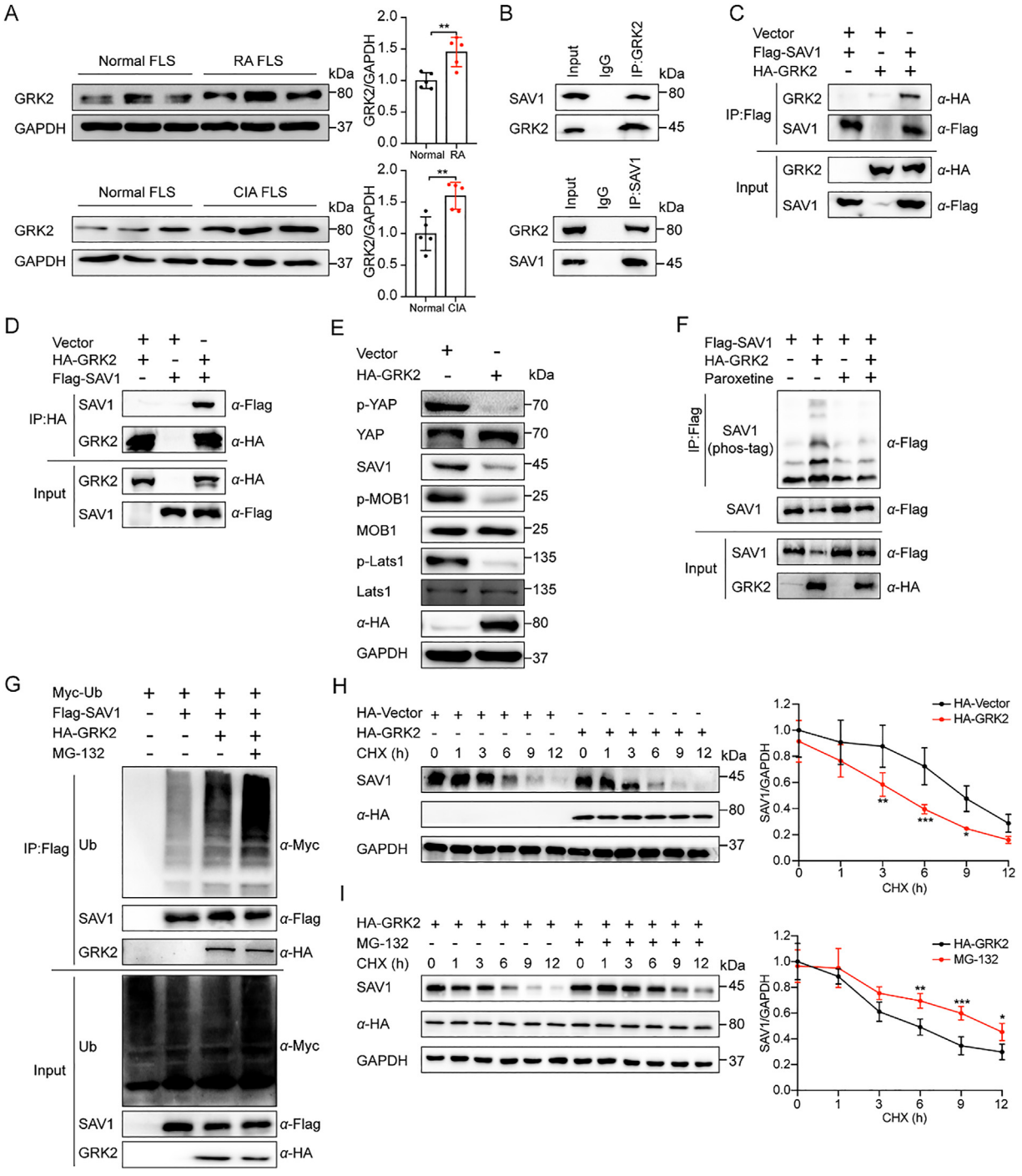

Figure 3 GRK2 promoted the phosphorylation and ubiquitin-mediated degradation of SAV1 in MH7A cells. (A) The protein expression of GRK2 in inflammatory FLSs was detected by immunoblotting ($n = 5$). All data were presented as mean ± SD and were analyzed by *t*-tests, $^{**}P < 0.01$. (B) Cell lysates from MH7A cells were immunoprecipitated with anti-GRK2 or anti-SAV1 antibodies, followed by immunoblotting with anti-GRK2 or anti-SAV1 antibodies. IgG was used as a control ($n = 3$). (C, D) Immunoblotting analysis was performed on lysates from MH7A cells transfected with Flag-SAV1 and HA-GRK2 after immunoprecipitation ($n = 3$). (E) MH7A cells were transfected with HA-vector or HA-GRK2 for 48 h, and immunoblotting was performed using antibodies against the indicated proteins ($n = 5$). (F) Flag-SAV1 or HA-GRK2 was overexpressed and treated with paroxetine (10 μmol/L) in MH7A cells. SAV1 phosphorylation was then determined by immunoblotting ($n = 3$). (G) Myc-ubiquitin and HA-GRK2 were simultaneously overexpressed and treated with MG-132 (10 μmol/L) in MH7A cells. SAV1 ubiquitination was then determined by immunoblotting ($n = 3$). (H) MH7A cells were transfected with HA vector or HA-GRK2 for 48 h. The cells were then treated with 10 μg/mL CHX and harvested at the indicated time points. SAV1 protein expression was assessed by immunoblotting ($n = 3$). (I) MH7A cells were transfected with HA-GRK2 and treated with MG-132 (10 μmol/L). The cells were then treated with 10 μg/mL CHX and harvested at the indicated time points. The SAV1 protein expression was assessed by immunoblotting ($n = 3$). All data were presented as mean ± SD and were analyzed by two-way ANOVA followed by a Tukey's post-test, $^{*}P < 0.05$, $^{**}P < 0.01$, $^{***}P < 0.001$.

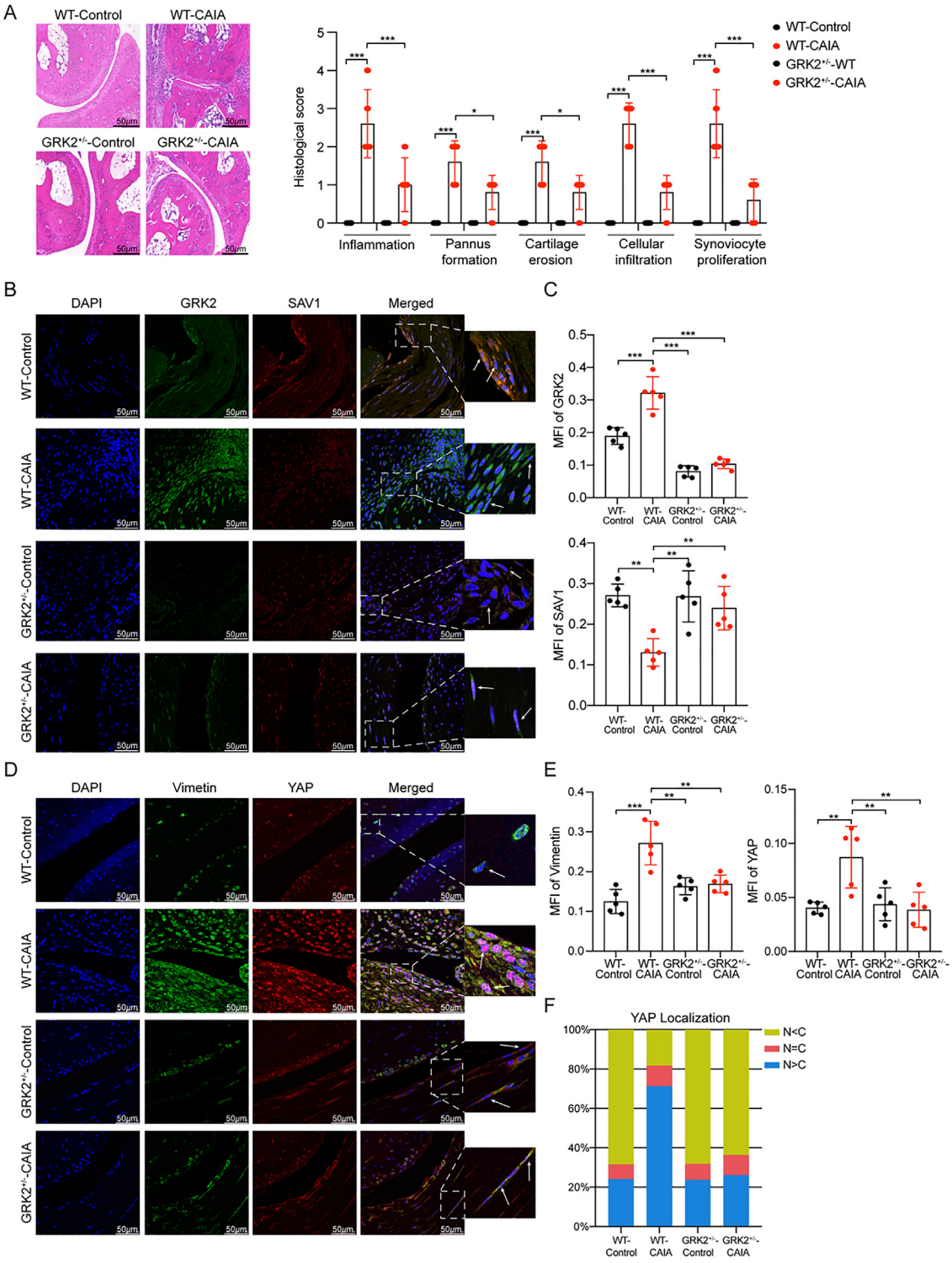

Figure 4 The deficiency of GRK2 in mice reduces the severity of inflammatory arthritis. (A) Representative H&E pathological images of ankle joints were presented, and graded analysis was conducted on pathological changes, including synovial hyperplasia, pannus formation, bone erosion, inflammation, and cellular infiltration ($n = 5$). Scale bar, 50 μm. (B) In paraffin sections of ankle tissues from CAIA mice, GRK2 was stained in green, and SAV1 was labeled in red. Images were taken by a confocal microscope. Scale bar, 50 μm. White arrow: positive GRK2 and SAV1 staining in FLSs. (C) The MFI of GRK2 and SAV1 was analyzed using ImageJ software ($n = 5$). (D) Ankle tissues from CAIA mice were sectioned and stained for vimentin (green) and YAP (red) using paraffin. A confocal microscope was used to capture the images. Scale bar, 50 μm. White arrow: positive vimentin and YAP staining in FLSs. (E) The MFI of Vimentin and YAP was analyzed using ImageJ software ($n = 5$). (F) The distribution analysis graph of YAP in 200 randomly selected cells was shown. All data were presented as mean ± SD, and were analyzed by one-way ANOVA followed by a Tukey's post-test, $^{*}P < 0.05$, $^{**}P < 0.01$, $^{***}P < 0.001$.

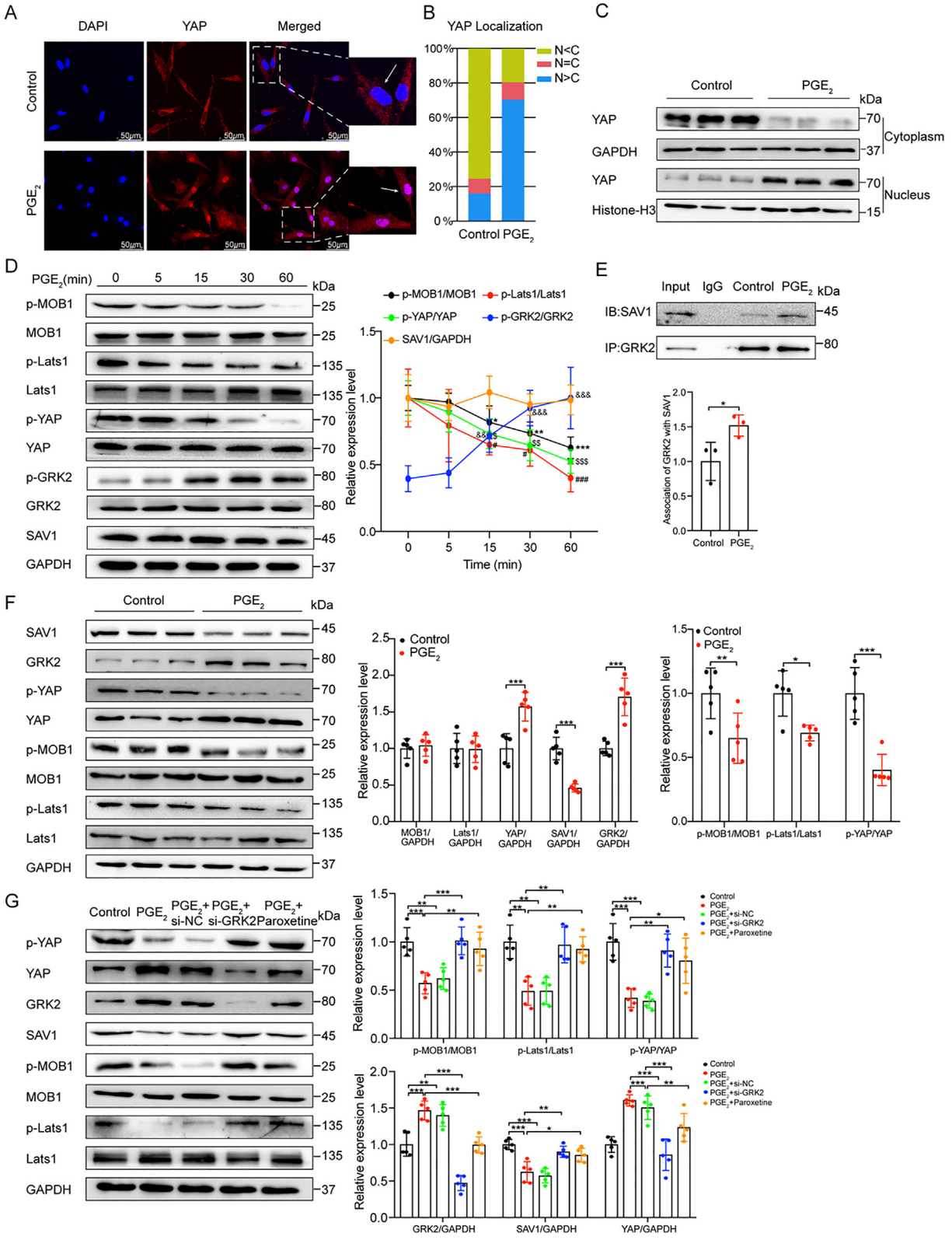

Figure 5 PGE_2 regulates YAP activation *via* GRK2 and is involved in FLSs proliferation and migration. (A) Rat FLSs were serum-starved for 24 h, treated with PGE_2 (5 μmol/L) for 24 h, and then subjected to immunofluorescence staining. YAP was stained in red and images were captured using a confocal microscope ($n = 5$). Scale bar, 50 μm. White arrow: positive YAP staining in FLSs. (B) The distribution analysis graph of YAP in 200 randomly selected cells was profiled. (C) Cytoplasmic and nuclear components were fractionated after treatment of rat FLSs with PGE_2 (5 μmol/L) for 24 h. The expression of YAP in the cytoplasm and nucleus was detected by immunoblotting ($n = 5$). (D) Rat FLSs were serum-starved for 24 h and treated with PGE_2 (5 μmol/L) for different time durations. Immunoblotting was performed using antibodies against the

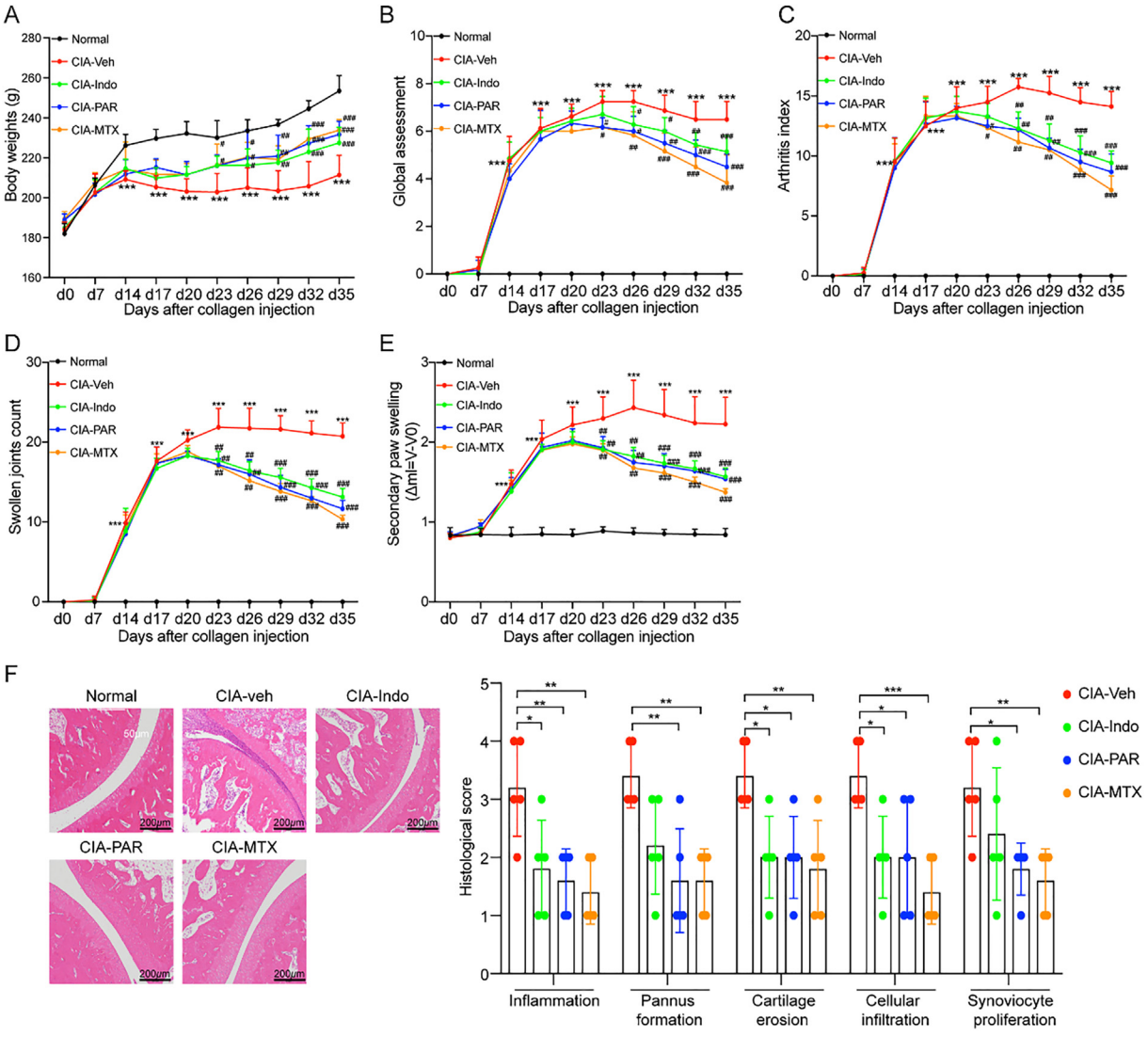

Figure 6 GRK2 inhibitor effectively improves the clinical manifestation of CIA rats. (A) Body weights. (B) Global assessment. (C) Arthritis index. (D) Swollen joints count. (E) Secondary paw swelling. The data were presented as mean ± SD and analyzed by two-way ANOVA followed by a Tukey's post-test, $^{***}P < 0.001$ *vs*. normal group, $^{\#}P < 0.05$, $^{\#\#}P < 0.01$; $^{\#\#\#}P < 0.001$ *vs*. CIA group, $n = 7-10$. (F) Representative H&E pathological images of ankle joints were analyzed for graded changes, including synovial hyperplasia, pannus formation, bone erosion, inflammation, and cell infiltration ($n = 5$). Scale bar, 200 μm. All data were presented as mean ± SD and were analyzed by one-way ANOVA followed by a Tukey's post-test, $^{*}P < 0.05$, $^{**}P < 0.01$, $^{***}P < 0.001$.

CHX chase assays were conducted in MH7A cells transfected with HA-GRK2. The results demonstrated that overexpression of GRK2 led to an accelerated degradation rate of SAV1 upon CHX treatment compared to the empty vector control (Fig. 3H). In contrast, MG-132 or paroxetine-treated GRK2-overexpressing cells exhibit a decelerated degradation rate of SAV1 relative to GRK2-overexpressing cells (Fig. 3I; Fig. S4C) indicating a ubiquitination and proteasome-dependent degradation of phosphorylated SAV1 by GRK2. Collectively, these results suggest that the interaction between GRK2 and SAV1 initiates phosphorylation, ubiquitination, and subsequent degradation of SAV1, turning off the Hippo pathway.

indicated proteins ($n = 5$). The data were presented as mean ± SD and analyzed by two-way ANOVA followed by a Tukey's post-test, $^{*}P < 0.05$, $^{**}P < 0.01$, $^{***}P < 0.001$ *vs*. 0 min (p-MOB1/MOB1); $^{\#}P < 0.05$, $^{\#\#\#}P < 0.001$ *vs*. 0 min (p-Lats1/Lats1); $^{\$}P < 0.05$, $^{\$\$}P < 0.01$, $^{\$\$\$}P < 0.001$ *vs*. 0 min (p-YAP/YAP); $^{\&\&}P < 0.01$, $^{\&\&\&}P < 0.001$ *vs*. 0 min (p-GRK2/GRK2). (E) Rat FLSs were pretreated with PGE_2 (5 μmol/L) for 1 h, and the interaction between SAV1 and GRK2 was evaluated ($n = 3$). All data were presented as mean ± SD and were analyzed by *t*-tests, $^{*}P < 0.05$. (F) Rat FLSs were serum-starved for 24 h and treated with PGE_2 (5 μmol/L) for 24 h. Immunoblotting was performed using antibodies against the indicated proteins ($n = 5$). (G) Rat FLSs treated with GRK2 siRNA or paroxetine (10 μmol/L) were then treated with PGE_2 (5 μmol/L) for 24 h. Immunoblotting was performed using antibodies against the indicated proteins ($n = 5$). All data were presented as mean ± SD and were analyzed by one-way ANOVA followed by a Tukey's post-test, $^{*}P < 0.05$, $^{**}P < 0.01$, $^{***}P < 0.001$.

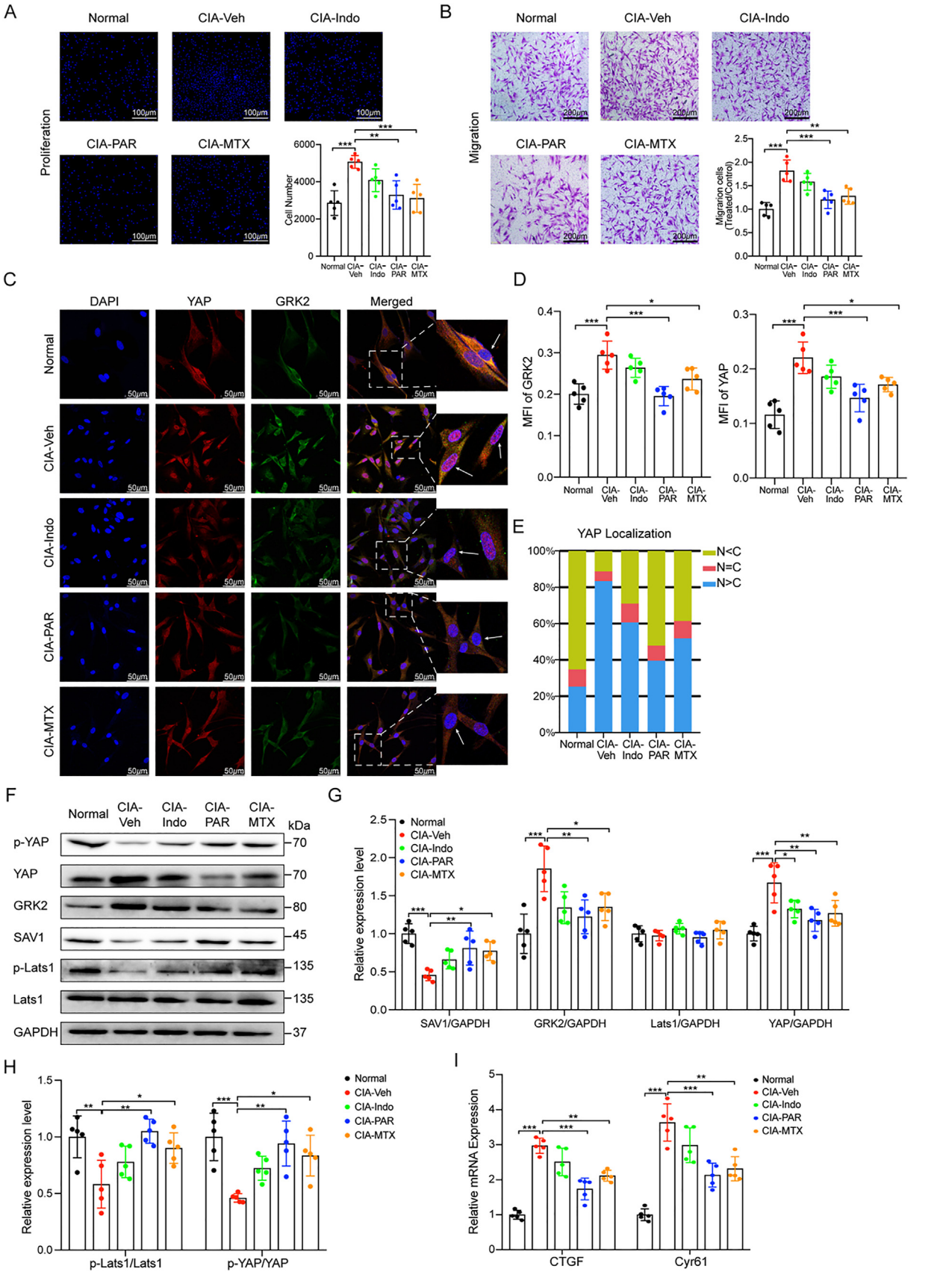

Figure 7 Paroxetine inhibits GRK2 and restores the Hippo-YAP signaling pathway. (A) For the FLSs of treated rats, nuclei were labeled with DAPI and captured using a high-content cell imager to count the number of cells ($n = 5$). Scale bar, 100 μm. (B) The FLSs of treated rats were visualized by crystal violet staining ($n = 5$). Scale bar, 200 μm. (C) For the FLSs of treated rats, GRK2 was stained in green and YAP was labeled

3.4. *Knockout of GRK2 prevents and reduces the severity of arthritis in the CAIA model*

To further illustrate the regulatory function of GRK2 in the Hippo-YAP pathway, $GRK2^{+/-}$ mice were utilized to establish a CAIA model. Histopathological examination of ankle joints in CAIA mice revealed joint space narrowing accompanied by synovial cell hyperproliferation, lymphocyte infiltration, and local inflammation. The deficiency of GRK2 significantly impeded synovial cell proliferation, lymphocyte infiltration, and inflammation (Fig. 4A). Namely, GRK2 haploinsufficiency had a significant inhibitory effect on the development of CAIA disease. The deficiency of GRK2 was examined for its effect on SAV1 expression within the ankle joint. SAV1 levels were significantly reduced in the WT-CAIA group compared with the WT-Control group. However, the heterozygosity of GRK2 restored SAV1 expression (Fig. 4B and C). In addition, the results of ankle joint fluorescence depicted that the MFI of Vimentin and YAP were significantly increased in the WT-CAIA group compared with the WT-Control group. Conversely, the MFI of Vimentin and YAP in $GRK2^{+/-}$CAIA was significantly reduced compared with the WT-CAIA group, and there was no significant difference between the WT-Control group (Fig. 4D and E). Furthermore, the localization of YAP in ankle FLSs was examined, and haploinsufficiency of GRK2 significantly reduced the nuclear localization of YAP in FLSs, which is consistent with the results from cultured cells (Fig. 4F). Altogether, these findings suggest that GRK2 plays a role in promoting FLSs proliferation, inflammation, and joint destruction by regulating the Hippo pathway.

3.5. *PGE_2 activates YAP via GRK2 to drive the aberrant proliferation of FLSs*

As a Ser/Thr kinase, GRK2 specifically phosphorylates GPCRs and mediates receptor desensitization. Our previous study revealed that in response to PGE_2 stimulation, the activity and transmembrane localization of GRK2 are enhanced, resulting in the desensitization of the Prostaglandin E receptor (EP), which plays a crucial role in the abnormal proliferation of FLSs[15]. PGE_2 is commonly used as a stimulant to investigate the functional properties of FLSs. Our previous findings have demonstrated that elevated concentrations of PGE_2 can effectively promote the proliferation and activation of FLSs *in vitro*[26]. Here, PGE_2 significantly promoted the proliferation and migration of FLSs in normal rats (Supporting Information Fig. S5A and S5B). Interestingly, PGE_2 markedly facilitated the nuclear localization of YAP, as seen by immunofluorescence and by immunoblotting of fractionations while promoting FLSs proliferation (Fig. 5A–C). Additionally, PGE_2 facilitated the upregulation of CTGF and Cyr61 mRNA levels (Fig. S5C). The impact of PGE_2 on the phosphorylation levels of constituents in the Hippo signaling pathway was then subsequently examined. PGE_2 acutely promoted the activation of GRK2 while exerting a time-dependent inhibitory effect on the phosphorylation of MOB1, Lats1, and YAP (Fig. 5D). The expression of SAV1 was not significantly changed in response to acute stimulation with PGE_2 (Fig. 5D), indicating that PGE_2 acute treatment would not affect the stability of SAV1. Meanwhile, PGE_2 acute stimulation promoted the combination between GRK2 and SAV1 (Fig. 5E). However, prolonged exposure to PGE_2 in rat FLSs resulted in decreased SAV1 levels and increased expression of GRK2 and YAP, with varying degrees of inhibition observed for the phosphorylation levels of MOB1, Lats1, and YAP (Fig. 5F). The classical downstream signaling pathway of PGE_2 involves the cyclic adenosine monophosphate-protein kinase A (PKA) pathway[28]. After treatment with a PKA inhibitor H89, there was no significant difference observed in YAP expression and activity compared to the PGE_2 group (Fig. S5D), indicating an insignificance of PKA in the system. Therefore, further investigation was focused on the effect of GRK2 on the Hippo-YAP pathway *in vitro*. Either GRK2-siRNA or paroxetine effectively inhibited PGE_2-induced proliferation and migration of FLSs (Supporting Information Fig. S6A–C). Reduction in expression or activity of GRK2 in rat FLSs resulted in altered phosphorylation patterns of MOB1, Lats1, and YAP, which led to the downregulation of YAP and upregulation of SAV1 (Fig. 5G). Moreover, GRK2-siRNA or paroxetine in rat FLSs resulted in the downregulation and cytoplasmic retention of YAP, as evidenced by immunofluorescence (Fig. S6D–F). Taken collectively, PGE_2 facilitates the degradation of SAV1 through GRK2-mediated mechanisms, resulting in reduced YAP phosphorylation and subsequent nuclear translocation, thereby contributing to the proliferation and migration of FLSs.

3.6. *Inhibition of GRK2 reduced the clinical parameters of CIA rats*

Since it has been demonstrated here that paroxetine reduces YAP expression *in vitro*, thereby inhibiting the proliferation of FLSs and previous work has revealed that indomethacin prevents spontaneous tumor formation in mice by suppressing YAP expression[29], the potential *in vivo* therapeutic benefits of paroxetine and indomethacin *via* modulation of the Hippo pathway was investigated in CIA rats. After d14 of CIA model induction, CIA rats were treated with indomethacin (2.5 mg/kg/day), paroxetine (15 mg/kg/day), and MTX (0.5 mg/kg/3 day) for 21 days. Compared to normal rats, CIA rats exhibited significantly lower body weight and more severe global assessment, arthritis index, swollen joints count, and secondary paw swelling. Indomethacin, paroxetine, and MTX exhibited varying degrees of efficacy in ameliorating the symptoms of CIA rats (Fig. 6A–E; Supporting Information Fig. S7A). Compared with normal rats, CIA rats exhibited splenomegaly and thymic atrophy. However, treatment with indomethacin, paroxetine, and MTX restored the size of both organs (Fig. S7B and S7C). Additionally, the ankle joints and toes of CIA rats were severely swollen compared to normal rats, with

in red. Images were captured using a confocal microscope. Scale bar, 50 μm. White arrow: positive GRK2 and YAP staining in FLSs. (D) The MFI of GRK2 and YAP was analyzed by ImageJ software ($n = 5$). (E) The distribution analysis graph of YAP in 200 randomly selected cells was plotted. (F) The expression and activity of Lats1, YAP, SAV1, and GRK2 in FLSs from treated rats were detected by Immunoblotting ($n = 5$). (G) The expressions of total proteins were analyzed. (H) The expressions of phosphorylated proteins were analyzed. (I) The transcription levels of the YAP downstream genes CTGF and Cyr61 were examined by real-time qPCR ($n = 5$). The data were presented as mean ± SD and analyzed by one-way ANOVA followed by a Tukey's post-test, $^*P < 0.05$, $^{**}P < 0.01$, $^{***}P < 0.001$.

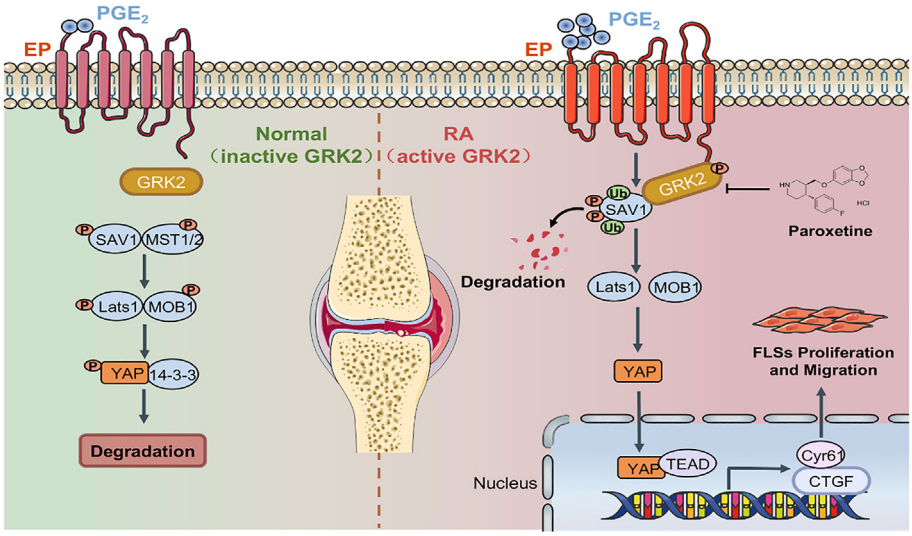

Figure 8 Schematic diagram depicting the mechanism by which GRK2 activates YAP to promote FLSs proliferation and migration. In normal joints, inactive GRK2 fails to promote SAV1 degradation, resulting in YAP phosphorylation and subsequent proteasomal degradation. While in RA FLSs with active GRK2, the interaction between GRK2 and SAV1 promotes SAV1 phosphorylation, ubiquitination, and degradation. This leads to an increase in un-phosphorylated Lats1, MOB1, and YAP, allowing the nuclear translocation of YAP and ultimately induces downstream gene expression, promoting RA FLSs proliferation and migration. Paroxetine prevents RA progression by inhibiting GRK2 activity.

X-rays revealing significant erosion in the bones of the ankle joints. Compared to the CIA rats, the treated groups effectively eliminated ankle joint and toe swelling, as well as inhibited bone erosion (Fig. S7D). Histological examination of the joints of CIA rats demonstrated that synovial cell hyperproliferation resulted in joint space narrowing, massive immune cell infiltration accompanied by pannus formation, marked cartilage erosion, and leukocyte aggregation. The treated groups significantly suppressed joint tissue inflammation, inflammatory cell infiltration, and bone tissue damage. Paroxetine and MTX exhibited significant inhibition of pannus formation and abnormal synovial cell proliferation, while indomethacin depicted insignificant inhibition of synovial cell proliferation and pannus formation (Fig. 6F).

3.7. Paroxetine down-regulates GRK2 expression to inhibit YAP nuclear translocation mediating abnormal FLSs proliferation

Synovial tissue was obtained from the knee joint of rats in each group, and FLSs were cultured using the tissue block adherence method. Aberrant FLSs proliferation was significantly increased in the CIA group compared to the control group, with paroxetine and MTX effectively suppressing aberrant proliferation and migration of FLSs (Fig. 7A and B). Immunofluorescence analysis revealed that the MFI of YAP and GRK2 were significantly increased in the CIA-Veh FLSs, accompanied by enhanced nuclear translocation of YAP. Compared with the CIA-Veh group, the paroxetine group significantly inhibited the MFI of GRK2 and YAP, as well as the nuclear translocation of YAP (Fig. 7C−E). Similarly, high expression of YAP and abundant nuclear distribution was observed in FLSs throughout the erosive injury sites when observed by in situ immunofluorescence and IHC staining of rat ankle joints from individual treatment groups. As expected, paroxetine alleviated the proliferation of FLSs while inhibiting the high expression and nuclear accumulation of YAP (Supporting Information Fig. S8A and S8B). To further investigate the impact of the tested drugs on components of Hippo signaling, immunoblotting was conducted. The results revealed that YAP and GRK2 protein levels were elevated in the CIA group, while MOB1, Lats1, and YAP activity as well as SAV1 expression were suppressed. Notably, treatment with paroxetine significantly increased both SAV1 protein levels and MOB1, Lats1, and YAP phosphorylation (Fig. 7F−H). In addition, qPCR results demonstrated significant enrichment of CTGF and Cyr61 in the CIA group, which was effectively attenuated by paroxetine (Fig. 7I). The above data indicate that YAP-mediated promotion of proliferation and migration in CIA FLSs is mediated by GRK2, and paroxetine may serve as an effective inhibitor to prevent RA progression in cases with high GRK2 expression. Thus, the aforementioned data present a molecular framework of GRK2 pathway activity that facilitates the proliferation and migration of RA FLSs, as illustrated in Fig. 8.

4. Discussion

The aberrant proliferation of FLSs is a crucial factor in inducing tissue damage and perpetuating inflammation in RA[30], but the molecular mechanisms involved in promoting FLSs proliferation remain to be completely understood. Therefore, inhibition of FLSs proliferation is considered a key therapeutic strategy intervention of RA. In the present study, it was discovered that GRK2 interacts with SAV1 and promotes SAV1 degradation, which in turn triggers YAP nuclear translocation and FLSs proliferation and migration, ultimately exacerbating arthritis severity. Furthermore, it was determined that the elimination of GRK2 ameliorates immune-mediated inflammatory arthritis by inhibiting SAV1 degradation and YAP nuclear input. Collectively, GRK2 regulates the proliferation and migration of FLSs through the SAV1-mediated Hippo-YAP signaling pathway. These results provide an important complement to the understanding of the mechanisms of FLSs hyperplasia and arthritis development.

SAV1 has long been recognized as a scaffolding protein, but its expression is reduced in various cancers and the mechanism of SAV1

reduction remains unclear[31]. One of the key findings here was that protein expression of SAV1 was significantly reduced in inflammatory FLSs, which was consistent with previous studies[19,20]. Recent cancer-related studies have determined that certain proteins (*e.g.*, BCL-2, P4HA2) interact with SAV1, leading to its ubiquitination and proteasomal degradation[32,33]. However, the regulatory molecules for SAV1 in RA FLSs remain unknown. When screening the previously reported interactor proteins including MST1/2 and AMOT, a large amount of GRK2 binds with SAV1. Moreover, it was then confirmed that over-expression of GRK2 resulted in decreased levels of the protein of SAV1, whereas knockdown and inhibition of GRK2 did the opposite. This study further demonstrated that GRK2 interacted with SAV1, leading to its phosphorylation, ubiquitination, and proteasomal degradation. This interaction inhibits YAP phosphorylation and cytoplasmic reduction, which leads to YAP's nuclear translocation and role as a transcriptional coactivator to prompt the expression of proliferation and migration genes, such as Cyr61 and CTGF. CTGF and Cyr61 have also been demonstrated to play a role in the pathophysiology of RA and are indispensable for the aggressive phenotype of FLSs[34,35]. The mass spectrometry data also revealed some other proteins that abundantly combined with SAV1. Many of these interacting proteins are highly upregulated in cancer. For instance, POTEE, PLEC, COL1A1, CALM1, SRSF10, KLHL22, and ABCF2, are involved in functions such as abnormal proliferation and migration of tumor cells[36], while LIMA1, GSTZ1, and SKIV2L2 are involved in the regulation of oxidative stress and energy metabolism[37]. There is a paucity of studies on SAV1, and understanding these protein interactions is essential for enriching comprehension of the regulatory mechanisms of the SAV1 or Hippo pathway.

In addition, it is well known that GRK2 phosphorylates numerous non-receptor substrates involved in the regulation of multiple cellular phenomena[13]. The current findings suggest that SAV1 is also a substrate for GRK2, although the exact site of phosphorylation remains unclear. So far, the deficiency of SAV1 has been reported in various kinds of tumors, and the regulatory mechanisms have been primarily described as gene mutation and epigenetic regulations. Here it was revealed that the phosphorylation of SAV1 could lead to its degradation through polyubiquitination. Accumulating data have indicated that most of the components in the Hippo signaling pathway are precisely regulated *via* proteasomal degradation through ubiquitination including MST1/2, TAZ, and YAP[38]. Of note, phosphorylation of Ser381 at YAP or Ser311 at TAZ leads to phosphodegron-induced, ubiquitination-mediated protein degradation[39,40]. The phosphodegron is a short linear motif in the substrate proteins that is activated by phosphorylation and subsequently interacts with a ubiquitin ligase[41]. As previously demonstrated, SAV1 is also the substrate of E3 ubiquitin ligase HERC4[42]. The phos-tag assay confirmed that GRK2 interacted with and phosphorylated SAV1, meanwhile, it promoted the degradation of SAV1 in a proteasome-dependent manner, suggesting that the degradation of SAV1 is mediated by phosphodegrons.

It has also been claimed that phosphorylation of GRK2 on S670 enables the phosphorylation of MST2 resulting in NIMA-related kinases 2A activation-induced centrosomal linker disassembly[43]. However, the phosphorylation of GRK2 at S670 is basically ERK-mediated. In PGE_2-stimulated FLSs, GRK2 is primarily phosphorylated at S685 by PKA[13]. This explains why an activation in MST2 and its downstream Hippo pathway, including the phosphorylation of Lats and YAP in the PGE_2-treated FLSs, was not observed. This also allows us to hypothesize that GRK2 may phosphorylate SAV1 by residue S685 in this system.

Accumulating evidence has revealed the crucial function of Hippo-YAP pathway dysregulation in RA[11,44]. For instance, YAP plays a specific role in pathological behavior associated with arthritis by promoting synovial angiogenesis and regulating vascular endothelial cell proliferation, migration, and survival[45]. Indeed, functional assays reported here determined that YAP promotes the proliferation and migration of FLSs *in vitro* and is involved in the development of inflammatory arthritis, which confirms the critical role of YAP in RA FLSs tumor-like proliferation. Various studies on RA disease have identified multiple pro-inflammatory cytokines (Interleukin-6, Interleukin-17, or TNF-α) that regulate the Hippo-YAP pathway[44,46]. Shreds of evidence have shown that cAMP-PKA signaling promotes the phosphorylation of YAP at serine 127 and leads to the degradation of YAP in hepatocellular carcinoma (HCC) cells[47]. In mouse cardiomyocytes, some GPCR agonists including isoproterenol phosphorylates both MST1 and YAP[48]. Alternatively, cAMP activates Lats first, then Lats phosphorylates YAP on Ser381 during neurological development[49]. Moreover, nuclear cAMP phosphorylates nuclear YAP at serine 397, resulting in the nuclear exclusion of YAP during tumorigenesis[50]. However, some studies have different conclusions. YAP inhibition could be resisted by cAMP-PKA-induced activation of ERK signaling in NF2-deficient tumor cells[51]. Also, cAMP-response element binding protein (CREB), an important downstream transcriptional factor of cAMP, promotes YAP expression and activation, exerting anti-apoptotic function in liver cancer or facilitating HCC proliferation[52,53]. In the present study, it was revealed that SAV1 was degraded by directly interacting with GRK2 under prolonged stimulation by PGE_2, and this process was not affected by PKA or cAMP demonstrating a novel crosstalk pattern between GPCR and Hippo signaling. Therefore, PGE_2 inhibits the phosphorylation levels of Lats1 and YAP in a time-dependent manner and promotes the expression and nuclear translocation of YAP. In addition, evidence has shown that distinct GPCR-cAMP signaling can trigger individual PKA isoforms type I and type II, which have different intracellular locations and functions[54]. This contradictory effect of PGE_2 and isoproterenol on YAP phosphorylation is probably because PGE_2 stimulation increases the activity of PKA isoforms type I, while isoproterenol activates PKA isoforms type II[55]. Alternatively, the role of numerous GPCR signals in the regulation of YAP in RA FLSs proliferation and even in other pathogenic factors of RA (*e.g.*, synovial angiogenesis, T helper cell subpopulation imbalance) remains to be investigated.

Although studies have demonstrated that VP treatment significantly reduces the severity of antigen-induced arthritis (AIA)[46], it should be noted that VP has YAP-independent cytostatic and highly cytotoxic effects, and previous research has denoted that its amelioration of AIA models is achieved through inducing immune cell apoptosis[56,57]. Indomethacin ameliorates some animal models of inflammation by inhibiting YAP-mediated COX-2 production[29,58]. However, in the current work, indomethacin was less effective than paroxetine and failed to significantly inhibit the proliferation of FLSs. Indomethacin inhibits COX-2 to reduce PGE_2 production, but it is weak in reducing GRK2 expression in CIA FLSs, since PGE_2 is not the only inducer of high GRK2 expression in an inflammatory environment[59,60]. This also suggests one of the possible reasons for the lack of effect of indomethacin in the clinical treatment of RA patients. Paroxetine is a well-known clinical antidepressant that also has a potent inhibitory effect on GRK2. Therefore, paroxetine was used to inhibit GRK2. GRK2 inhibition blocked inflammation-induced

YAP activation, effectively preventing the proliferation of inflammatory FLSs. The potential side effects of paroxetine on the central nervous system have limited its use in clinical practice for GRK2 inhibition. Several GRK2 inhibitors with milder side effects are in preclinical trials due to the importance of GRK2 in many diseases[61]. Further refinement of the network of regulatory mechanisms of GRK2 is essential for basic science and translational applications. The Hippo-YAP signaling pathway presents an attractive target for disease treatment, but a challenge in this area is the lack of a well-established cell surface marker or regulator as a therapeutic target. Results presented here suggest that targeting GRK2 to restore the balance of the Hippo-YAP pathway may be an effective strategy to inhibit FLSs proliferation and ameliorate arthritis. Hence, there is an urgent need to conduct further research and develop novel drugs that specifically target GRK2 for the treatment of RA.

5. Conclusions

Data presented here demonstrate the physiological significance of GRK2-SAV1 interaction in regulating YAP. We report a novel PGE_2-GRK2-SAV1-YAP signaling axis that links inflammation mediated by inflammatory factors to tumor-like proliferation of RA FLSs. GRK2 was identified as a novel regulator of the Hippo-YAP pathway in RA FLSs proliferation and migration. These results accentuate a meaningful clinical application of targeting the GRK2-mediated Hippo-YAP pathway for treating RA.

Acknowledgments

This work was supported by the National Natural Science Foundation of China (81973314, 82373865, 81973332, 82173824), the Anhui Provincial Natural Science Foundation for Distinguished Young Scholars (1808085J28, China), Collaborative Innovation Project of Key Scientific Research Platform in Anhui Universities (GXXT-2020-066, China), the Research Program for Higher Education Institutions in Anhui Province (2022AH030081, China), Anhui Provincial Key R&D Programs (2022e07020042, China), Program for Upgrading Scientific Research Level of Anhui Medical University (2019xkjT008, China) and Academic Funding for Top-notch Talents in University Disciplines (Majors) of Anhui Province (gxbjZD2021047, China).

Author contributions

Paipai Guo, Qingtong Wang, Wei Wei, and Shihao Zhang designed the research. Ji Jiang completed the experiments for revision. Paipai Guo, Ji Jiang, Rui Chu, Huijuan Cheng, Tiantian Su, Feng He, Mingli Ge, Ruhong Fang, and Qiuyun Guan conducted most of the experiments. Chunru Jiang and Zhenduo Zhu analyzed the data and produced figures. Hao Liu revised the manuscript. Wei Wei, Shihao Zhang and Qingtong Wang obtained funding and supervised the entire project. The manuscript has been reviewed and approved by all authors.

Conflicts of interest

The authors declare no conflicts of interest.

Appendix A. Supporting information

Supporting data to this article can be found online at https://doi.org/10.1016/j.apsb.2023.12.007.

References

1. Nygaard G, Firestein GS. Restoring synovial homeostasis in rheumatoid arthritis by targeting fibroblast-like synoviocytes. *Nat Rev Rheumatol* 2020;**16**:316–33.
2. Loh C, Park SH, Lee A, Yuan R, Ivashkiv LB, Kalliolias GD. TNF-induced inflammatory genes escape repression in fibroblast-like synoviocytes: transcriptomic and epigenomic analysis. *Ann Rheum Dis* 2019;**78**:1205–14.
3. Emori T, Kasahara M, Sugahara S, Hashimoto M, Ito H, Narumiya S, et al. Role of JAK-STAT signaling in the pathogenic behavior of fibroblast-like synoviocytes in rheumatoid arthritis: effect of the novel JAK inhibitor peficitinib. *Eur J Pharmacol* 2020;**882**:173238.
4. Kondo N, Kuroda T, Kobayashi D. Cytokine networks in the pathogenesis of rheumatoid arthritis. *Int J Mol Sci* 2021;**22**:10922.
5. Zhao J, Guo S, Schrodi SJ, He D. Molecular and cellular heterogeneity in rheumatoid arthritis: mechanisms and clinical implications. *Front Immunol* 2021;**12**:790122.
6. Jia XY, Chang Y, Sun XJ, Dai X, Wei W. The role of prostaglandin E2 receptor signaling of dendritic cells in rheumatoid arthritis. *Int Immunopharmacol* 2014;**23**:163–9.
7. de Sousa N, Rodriguez-Esteban G, Rojo-Laguna JI, Salo E, Adell T. Hippo signaling controls cell cycle and restricts cell plasticity in planarians. *PLoS Biol* 2018;**16**:e2002399.
8. de Amorim ISS, Dias IX, Pinheiro D, de Carvalho SN, Nicolau-Neto P, Rodrigues JA, et al. Profiles of expression of SAV1 in normoxia or hypoxia microenvironment are associated with breast cancer prognosis. *Arch Med Res* 2023;**54**:79–85.
9. Han H, Nakaoka HJ, Hofmann L, Zhou JJ, Yu C, Zeng L, et al. The Hippo pathway kinases LATS1 and LATS2 attenuate cellular responses to heavy metals through phosphorylating MTF1. *Nat Cell Biol* 2022;**24**:74–87.
10. Roelofs AJ, Zupan J, Riemen AHK, Kania K, Ansboro S, White N, et al. Joint morphogenetic cells in the adult mammalian synovium. *Nat Commun* 2017;**8**:15040.
11. Bottini A, Wu DJ, Ai R, Le Roux M, Bartok B, Bombardieri M, et al. PTPN14 phosphatase and YAP promote TGFbeta signalling in rheumatoid synoviocytes. *Ann Rheum Dis* 2019;**78**:600–9.
12. de Amorim ISS, de Sousa Rodrigues MM, Mencalha AL. The tumor suppressor role of salvador family WW domain-containing protein 1 (SAV1): one of the key pieces of the tumor puzzle. *J Cancer Res Clin Oncol* 2021;**147**:1287–97.
13. Penela P, Ribas C, Sanchez-Madrid F, Mayor Jr F. G protein-coupled receptor kinase 2 (GRK2) as a multifunctional signaling hub. *Cell Mol Life Sci* 2019;**76**:4423–46.
14. Nogues L, Palacios-Garcia J, Reglero C, Rivas V, Neves M, Ribas C, et al. G protein-coupled receptor kinases (GRKs) in tumorigenesis and cancer progression: GPCR regulators and signaling hubs. *Semin Cancer Biol* 2018;**48**:78–90.
15. Han C, Li Y, Zhang Y, Wang Y, Cui D, Luo T, et al. Targeted inhibition of GRK2 kinase domain by CP-25 to reverse fibroblast-like synoviocytes dysfunction and improve collagen-induced arthritis in rats. *Acta Pharm Sin B* 2021;**11**:1835–52.
16. Wang Q, Wang L, Wu L, Zhang M, Hu S, Wang R, et al. Paroxetine alleviates T lymphocyte activation and infiltration to joints of collagen-induced arthritis. *Sci Rep* 2017;**7**:45364.
17. Han CC, Liu Q, Zhang Y, Li YF, Cui DQ, Luo TT, et al. CP-25 inhibits PGE2-induced angiogenesis by down-regulating EP4/AC/cAMP/PKA-mediated GRK2 translocation. *Clin Sci* 2020;**134**:331–47.

18. Tu J, Chen W, Fang Y, Han D, Chen Y, Jiang H, et al. PU.1 promotes development of rheumatoid arthritis *via* repressing FLT3 in macrophages and fibroblast-like synoviocytes. *Ann Rheum Dis* 2023;**82**:198−211.
19. Woetzel D, Huber R, Kupfer P, Pohlers D, Pfaff M, Driesch D, et al. Identification of rheumatoid arthritis and osteoarthritis patients by transcriptome-based rule set generation. *Arthr Res Ther* 2014;**16**:R84.
20. Ungethuem U, Haeupl T, Witt H, Koczan D, Krenn V, Huber H, et al. Molecular signatures and new candidates to target the pathogenesis of rheumatoid arthritis. *Physiol Genom* 2010;**42A**:267−82.
21. Piccolo S, Dupont S, Cordenonsi M. The biology of YAP/TAZ: hippo signaling and beyond. *Physiol Rev* 2014;**94**:1287−312.
22. Dey A, Varelas X, Guan KL. Targeting the Hippo pathway in cancer, fibrosis, wound healing and regenerative medicine. *Nat Rev Drug Discov* 2020;**19**:480−94.
23. Liu Y, Lu T, Zhang C, Xu J, Xue Z, Busuttil RW, et al. Activation of YAP attenuates hepatic damage and fibrosis in liver ischemia-reperfusion injury. *J Hepatol* 2019;**71**:719−30.
24. Lin Z, Xie R, Guan K, Zhang M. A WW tandem-mediated dimerization mode of SAV1 essential for Hippo signaling. *Cell Rep* 2020;**32**:108118.
25. Mana-Capelli S, McCollum D. Angiomotins stimulate LATS kinase autophosphorylation and act as scaffolds that promote Hippo signaling. *J Biol Chem* 2018;**293**:18230−41.
26. Jia XY, Chang Y, Wei F, Dai X, Wu YJ, Sun XJ, et al. CP-25 reverses prostaglandin E4 receptor desensitization-induced fibroblast-like synoviocyte dysfunction *via* the G protein-coupled receptor kinase 2 in autoimmune arthritis. *Acta Pharmacol Sin* 2019;**40**:1029−39.
27. Thal DM, Homan KT, Chen J, Wu EK, Hinkle PM, Huang ZM, et al. Paroxetine is a direct inhibitor of g protein-coupled receptor kinase 2 and increases myocardial contractility. *ACS Chem Biol* 2012;**7**:1830−9.
28. Wehbi VL, Tasken K. Molecular mechanisms for cAMP-mediated immunoregulation in T cells − role of anchored protein kinase A signaling units. *Front Immunol* 2016;**7**:222.
29. Kim HB, Kim M, Park YS, Park I, Kim T, Yang SY, et al. Prostaglandin E2 activates YAP and a positive-signaling loop to promote colon regeneration after colitis but also carcinogenesis in mice. *Gastroenterology* 2017;**152**:616−30.
30. Falconer J, Murphy AN, Young SP, Clark AR, Tiziani S, Guma M, et al. Review: synovial cell metabolism and chronic inflammation in rheumatoid arthritis. *Arthr Rheumatol* 2018;**70**:984−99.
31. Zhao Z, Xiang S, Qi J, Wei Y, Zhang M, Yao J, et al. Correction of the tumor suppressor salvador homolog-1 deficiency in tumors by lycorine as a new strategy in lung cancer therapy. *Cell Death Dis* 2020;**11**:387.
32. Won GW, Park SH, Park J, Lee Y, Lee YH. Mammalian Hippo kinase pathway is downregulated by BCL-2 *via* protein degradation. *Biochem Biophys Res Commun* 2019;**512**:87−92.
33. Zhang J, Lyu Z, Li B, You Z, Cui N, Li Y, et al. P4HA2 induces hepatic ductular reaction and biliary fibrosis in chronic cholestatic liver diseases. *Hepatology* 2023;**78**:10−25.
34. Huang TL, Mu N, Gu JT, Shu Z, Zhang K, Zhao JK, et al. DDR2-CYR61-MMP1 signaling pathway promotes bone erosion in rheumatoid arthritis through regulating migration and invasion of fibroblast-like synoviocytes. *J Bone Miner Res* 2017;**32**:407−18.
35. Liu SC, Chuang SM, Hsu CJ, Tsai CH, Wang SW, Tang CH. CTGF increases vascular endothelial growth factor-dependent angiogenesis in human synovial fibroblasts by increasing miR-210 expression. *Cell Death Dis* 2014;**5**:e1485.
36. Shen Z, Feng X, Fang Y, Li Y, Li Z, Zhan Y, et al. POTEE drives colorectal cancer development *via* regulating SPHK1/p65 signaling. *Cell Death Dis* 2019;**10**:863.
37. Zhang YY, Fu ZY, Wei J, Qi W, Baituola G, Luo J, et al. A LIMA1 variant promotes low plasma LDL cholesterol and decreases intestinal cholesterol absorption. *Science* 2018;**360**:1087−92.
38. Deng L, Meng T, Chen L, Wei W, Wang P. The role of ubiquitination in tumorigenesis and targeted drug discovery. *Signal Transduct Target Ther* 2020;**5**:11.
39. Zhao B, Li L, Tumaneng K, Wang CY, Guan KL. A coordinated phosphorylation by Lats and CK1 regulates YAP stability through SCF(beta-TRCP). *Genes Dev* 2010;**24**:72−85.
40. Liu CY, Zha ZY, Zhou X, Zhang H, Huang W, Zhao D, et al. The hippo tumor pathway promotes TAZ degradation by phosphorylating a phosphodegron and recruiting the SCFbeta-TrCP E3 ligase. *J Biol Chem* 2010;**285**:37159−69.
41. Zhang B, Liu Q, Wen W, Gao H, Wei W, Tang A, et al. The chromatin remodeler CHD6 promotes colorectal cancer development by regulating TMEM65-mediated mitochondrial dynamics *via* EGF and Wnt signaling. *Cell Discov* 2022;**8**:130.
42. Huang F, Tang X, Sun T, Wang G, Ru Q, Zheng Y. SAV1, regulated by HERC4, inhibits the proliferation, migration, and invasion of hepatocellular carcinoma. *Transl Cancer Res* 2021;**10**:349−60.
43. Reglero C, Ortiz Del Castillo B, Rivas V, Mayor Jr F, Penela P. Mdm2-mediated downmodulation of GRK2 restricts centrosome separation for proper chromosome congression. *Cells* 2021;**10**:729.
44. Symons RA, Colella F, Collins FL, Rafipay AJ, Kania K, McClure JJ, et al. Targeting the IL-6-Yap-Snail signalling axis in synovial fibroblasts ameliorates inflammatory arthritis. *Ann Rheum Dis* 2022;**81**:214−24.
45. Chen Q, Fan K, Chen X, Xie X, Huang L, Song G, et al. Ezrin regulates synovial angiogenesis in rheumatoid arthritis through YAP and Akt signalling. *J Cell Mol Med* 2021;**25**:9378−89.
46. Caire R, Audoux E, Courbon G, Michaud E, Petit C, Dalix E, et al. YAP/TAZ: key players for rheumatoid arthritis severity by driving fibroblast like synoviocytes phenotype and fibro-inflammatory response. *Front Immunol* 2021;**12**:791907.
47. Ren H, Chen Y, Ao Z, Cheng Q, Yang X, Tao H, et al. PDE4D binds and interacts with YAP to cooperatively promote HCC progression. *Cancer Lett* 2022;**541**:215749.
48. Ashokkumar R, Jamuna S, Sakeena Sadullah MS, Niranjali Devaraj S. Vitexin protects isoproterenol induced post myocardial injury by modulating hipposignaling and ER stress responses. *Biochem Biophys Res Commun* 2018;**496**:731−7.
49. Kim M, Kim M, Lee S, Kuninaka S, Saya H, Lee H, et al. cAMP/PKA signalling reinforces the LATS-YAP pathway to fully suppress YAP in response to actin cytoskeletal changes. *EMBO J* 2013;**32**:1543−55.
50. Drozdz MM, Doane AS, Alkallas R, Desman G, Bareja R, Reilly M, et al. A nuclear cAMP microdomain suppresses tumor growth by Hippo pathway inactivation. *Cell Rep* 2022;**40**:111412.
51. White SM, Avantaggiati ML, Nemazanyy I, Di Poto C, Yang Y, Pende M, et al. YAP/TAZ inhibition induces metabolic and signaling rewiring resulting in targetable vulnerabilities in NF2-deficient tumor cells. *Dev Cell* 2019;**49**:425−43.e9.
52. Ma L, Wang J, Lin J, Pan Q, Yu Y, Sun F. Cluster of differentiation 166 (CD166) regulated by phosphatidylinositide 3-kinase (PI3K)/AKT signaling to exert its anti-apoptotic role *via* yes-associated protein (YAP) in liver cancer. *J Biol Chem* 2014;**289**:6921−33.
53. Yang S, Jiang W, Yang W, Yang C, Yang X, Chen K, et al. Epigenetically modulated miR-1224 suppresses the proliferation of HCC through CREB-mediated activation of YAP signaling pathway. *Mol Ther Nucl Acids* 2021;**23**:944−58.
54. Raslan Z, Magwenzi S, Aburima A, Tasken K, Naseem KM. Targeting of type I protein kinase A to lipid rafts is required for platelet inhibition by the 3′,5′-cyclic adenosine monophosphate-signaling pathway. *J Thromb Haemost* 2015;**13**:1721−34.
55. Di Benedetto G, Zoccarato A, Lissandron V, Terrin A, Li X, Houslay MD, et al. Protein kinase A type I and type II define distinct intracellular signaling compartments. *Circ Res* 2008;**103**:836−44.
56. Nguyen CDK, Yi C. YAP/TAZ signaling and resistance to cancer therapy. *Trends Cancer* 2019;**5**:283−96.
57. Zhang H, Ramakrishnan SK, Triner D, Centofanti B, Maitra D, Gyorffy B, et al. Tumor-selective proteotoxicity of verteporfin inhibits colon cancer progression independently of YAP1. *Sci Signal* 2015;**8**:ra98.
58. Yao L, He J, Li B, Yan M, Wang H, Tan L, et al. Regulation of YAP by mammalian target of rapamycin complex 1 in endothelial cells

controls blood pressure through COX-2/mPGES-1/PGE(2) cascade. *Hypertension* 2019;**74**:936−46.

59. Arraes SM, Freitas MS, da Silva SV, de Paula Neto HA, Alves-Filho JC, Auxiliadora Martins M, et al. Impaired neutrophil chemotaxis in sepsis associates with GRK expression and inhibition of actin assembly and tyrosine phosphorylation. *Blood* 2006;**108**: 2906−13.
60. Vila-Bedmar R, Cruces-Sande M, Arcones AC, Willemen H, Prieto P, Moreno-Indias I, et al. GRK2 levels in myeloid cells modulate adipose-liver crosstalk in high fat diet-induced obesity. *Cell Mol Life Sci* 2020;**77**:4957−76.
61. Zhang Y, Zhang J, Wang J, Chen H, Ouyang L, Wang Y. Targeting GRK2 and GRK5 for treating chronic degenerative diseases: advances and future perspectives. *Eur J Med Chem* 2022;**243**:114668.